Transportation Geotechnics 46 (2024) 101260

Contents lists available at ScienceDirect

Transportation Geotechnics

journal homepage: www.elsevier.com/locate/trgeo

Original Article

Self-sensing cementitious geocomposites in rail track substructures

António Gomes Correia *, Mohammad Jawed Roshan

University of Minho, ISISE, ARISE, Department of Civil Engineering, 4800-058 Guimarães, Portugal

ARTICLE INFO

Keywords:
Self-sensing
Geocomposite
MWCNTs/GNPs
Resilient modulus
Degree of saturation
Railways

ABSTRACT

A self-sensing cementitious geocomposite was developed based on laboratory data, and it demonstrated good physical and mechanical properties, durability, and piezoresistivity performance. It consisted of stabilized cemented sand containing multiwalled carbon nanotubes (MWCNTs) with graphene nanoplatelets (GNPs) as conductive fillers. This geocomposite could be used to detect damage based on the relationship between electrical impedance and mechanical performance, making it suitable for use as structural layers in railway lines. In this study, the effects of MWCNTs and GNPs, as well as of degree of saturation, were evaluated on the compaction, secant modulus, resilient modulus, electrical resistance, and piezoresistivity of the geocomposite. Scanning electron microscopy (SEM) and microscopic imaging were used to analyse microstructural alterations induced by varying concentrations of MWCNTs and GNPs. This innovative geocomposite, intended for installation in Portuguese railway lines as part of the EU project IN2TRACK3, is aimed at capturing performance data, identifying structural damage levels, and estimating load intensity, axle numbers, and train speed. The feasibility of its use is discussed based on literature studies and research conducted under the IN2TRACK2 and IN2TRACK3 projects, and its potential advantages over traditional methods for monitoring rail track health are highlighted.

Introduction

The stability of railway track hinges upon the stability of each individual layer and elements. Specifically, the subgrade serves as the foundational layer for all upper layers, underscoring its pivotal role in ensuring the overall track stability [1]. Consequently, efforts have been directed towards stabilizing the subgrade layer, with widespread utilization of both calcium-based and non-calcium-based stabilizers [2]. Cement, among the various calcium-based stabilizers, has emerged as a prominent choice for subgrade soil stabilization due to its ready availability in the market, high resistance against environmental stresses such as freeze–thaw and wetting–drying cycles, and suitability for diverse soil types. To date, extensive research has been conducted on cement stabilized soils, encompassing investigations into their index characteristics, advanced geotechnical properties, and microstructural attributes. However, traditional cement stabilized soils primarily exhibit structural features, leading to improvements in geotechnical characteristics solely. To enhance these soils with nonstructural features alongside their structural counterparts, the incorporation of carbon nanomaterials (CNMs) presents a promising advantage [3]. The intrinsic self-sensing geocomposite generated through the integration of CNMs has the potential to be efficacious for the structural health monitoring (SHM) of railway tracks.

Conventional instrumentation for SHM faces several challenges, including localized monitoring, maintenance difficulties, the excessive number of sensors required, challenges in sensor installation, detachment of external sensors from host materials, low sensor reliability and durability, the adverse effects of external sensors on host materials, and high costs [4]. In response to these challenges, the development of intrinsic self-sensing cementitious composites offers a promising solution, potentially overcoming the limitations of conventional instrumentation in SHM.

To date, extensive evaluations have been conducted on the influence of various types of CNMs, including GNPs, carbon fibers (CFs), carbon

Abbreviations: CSH, Calcium silicate hydrate; CAH, Calcium aluminate hydrate; CVD, chemical vapor deposition; CNMs, Carbon nanomaterials; CFs, Carbon fibers; CNFs, Carbon nanofibers; CNTs, Carbon nanotubes; CEL, Specific Energy Level; DIC, Digital image correlation; FCR, Fractional changes in resistivity/resistance; GNPs, Graphene nanoplatelets; G, Gauge factor; HSR, High-speed railway; MWCNTs, Multi-walled carbon nanotubes; OMC, Optimum moisture content; OPC, Ordinary Portland cement; PSD, Particle size distribution; SEM, Scanning electron microscopy; SWCC, Soil water characteristic curve; SHM, Structural health monitoring; UCS, Unconfined compressive strength; UGM, Unbound granular materials.

* Corresponding author.
E-mail address: agc@civil.uminho.pt (A. Gomes Correia).

https://doi.org/10.1016/j.trgeo.2024.101260
Received 23 March 2024; Received in revised form 23 April 2024; Accepted 24 April 2024
Available online 26 April 2024
2214-3912/© 2024 The Authors. Published by Elsevier Ltd. This is an open access article under the CC BY license (http://creativecommons.org/licenses/by/4.0/).

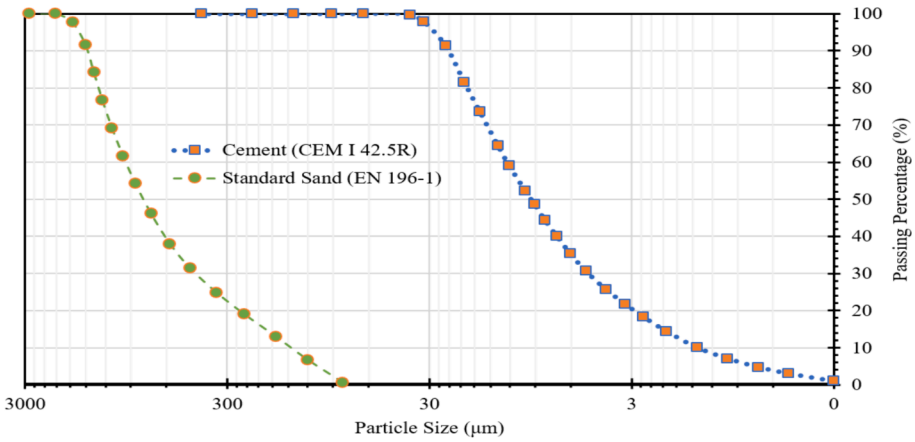


Fig. 1. Particle size distribution of sand and cement.

nanofibers (CNFs), and carbon nanotubes (CNTs), on the structural and non-structural properties of cementitious composites such as self-sensing cement paste, self-sensing mortar, and self-sensing concrete [5,6,7]. However, there remains a gap in the literature regarding the thorough exploration of CNMs' effects on the structural and non-structural properties of cement-stabilized soils [8,9,10]. Self-sensing cement-stabilized sand, augmented with multi-walled carbon nanotubes (MWCNTs) and GNPs, has been developed to autonomously detect stress, strain, and damage under both monotonic and cyclic loading conditions [11]. Digital image correlation (DIC) was employed to validate the sensing capabilities of self-sensing cement-stabilized sand subjected to cyclic loading. Additionally, in another study, DIC was utilized to confirm the effectiveness of a novel approach proposed for detecting damage in self-sensing cement-stabilized sand enhanced with MWCNTs/GNPs [3].

Among the various geotechnical properties of cement-stabilized sand, compaction is a pivotal parameter that is crucial for subgrade construction and quality control [12,13,14]. Replication of field compaction in laboratory settings is achieved through controlled mechanical energy input following a methodology proposed by Proctor in 1933 [15]. During compaction, the density of layers increases while air voids diminish due to the rearrangement of soil particles, leading to reduced settlement, hydraulic conductivity, and increased shear strength, shear modulus, and bearing capacity [16,17]. However, studies have shown that the small strain shear modulus initially increases with increasing compaction at a specific water content. After reaching the peak point of the compaction curve, however, the small strain shear modulus decreases with further increases in compaction efforts at the same water content. This suggests that the increase in small strain shear modulus is not solely dependent on dry density of the medium [18]. Consequently, the compaction quality of layers during construction significantly impacts the quality, durability, and overall performance of transportation infrastructures throughout their service lifespan [19]. Several factors, including soil type, moisture content, degree of saturation, compaction energy, environmental conditions, and additives, influence the compaction characteristics of soils [20,21]. Previous research has shown an increase in the maximum dry density ($(\rho_d)_{max}$) of stabilized soils with increasing cement content [22]. Conversely, the optimum moisture content (OMC) exhibits two distinct variation patterns with increasing cement content. Some studies have reported an increase in OMC with cement content due to moisture absorption by cement particles [23], while others have observed a decreasing trend in OMC with cement content owing to an increase in density and a decrease in voids [24]. In addition to compaction, the resilient modulus of cement-stabilized soil is a critical parameter that reflects the stiffness of the soil under cyclic traffic loading [25]. Furthermore, the resilient modulus of subgrade soil, which reflects soil stiffness characteristics, serves as a key input parameter in the structural design of railway tracks.

The variation in the resilient modulus is contingent upon various factors encompassing soil properties (such as soil type, gradation, moisture content, dry density, degree of saturation, and shear strength) as well as stress state and stress level (including bulk stress, confining pressure, and deviator stress) [26,27]. In previous research, the influence of these factors on the resilient modulus of various soil types has been extensively examined [28,29].

While the impact of cement content on the geotechnical characteristics of soils has been extensively investigated in previous studies, as detailed information in a review paper [30], the influence of CNMs content on the structural and nonstructural properties of cement-stabilized soil has not been thoroughly addressed in the literature. Therefore, in this research, the aim was to examine the effects of MWCNTs and GNPs contents on the compaction, secant deformability modulus, resilient modulus, electrical resistance, and piezoresistivity of 10 % cement stabilized sand. Additionally, the relationship between the content of MWCNTs/GNPs and the degree of saturation and between the degree of saturation and the resilient modulus were investigated. Furthermore, microstructural analysis was conducted to provide a good understanding of the influence of MWCNTs/GNPs on the cement-stabilized sand. To assess the potential for deployment of engineered self-sensing cement-stabilized sand in practical projects, the authors also examined the suitability of the self-sensing cementitious geocomposites for integration into transportation infrastructures, mainly in railway tracks, drawing upon insights from the literature.

Materials and methods

Materials

In this study, standard sand was utilized to mitigate the influence of soil gradation effects on both mechanical and electromechanical outcomes. The gradation curve of the standard sand employed in this study is depicted in Fig. 1. Cement is a commonly employed stabilization agent for subgrade soil due to its practicality and resilience against traffic and environmental loads. Therefore, ordinary Portland cement (OPC) CEM 42.5R was chosen for this study owing to its ready availability on the market and its alignment with geotechnical and European standards (ISO 679:2009 and EN 196–1). The particle size distribution (PSD) of the utilized cement is illustrated in Fig. 1. While various percentages of cement have been utilized in previous studies for the stabilization of different soils [30], a 10 % cement content was selected for this study due to its adequacy in achieving the required mechanical strength within established standards.

One of the primary objectives of this study was to assess the impact of

Table 1
Characteristics of GNPs and MWCNTs.

GNPs					
Surface Area ($m^2\ g^{-1}$)	Density (g/cm^3)	Carbon Content (%)	Tensile Modulus (GPa)	PH Value (30°C)	Tensile Strength (GPa)
120–150	0.6	>99.5	1000	7–7.65	5
Layers	Dimension		Form	Part Number	
10 < n < 60	Thickness 4–60 nm	Diameter 5–10 μm	Gray Powder	TGN201	
MWCNTs					
Surface Area ($m^2\ g^{-1}$)		Density (g/cm^3)	Color	Outside Diameter (nm)	
350		0.27	Black	<50	
Length (μm)	Ash (wt. %)		Carbon Content (%)		Part Number
10–30	<1.5		>98		GCM327

different percentages of CNMs on the mechanical and electromechanical properties of 10 % cement-stabilized sand. To achieve this goal, a hybrid mixture of MWCNTs and GNPs (at equal proportion 1:1) was considered at various percentage by weight of dry sand (i.e., 0.5 %, 1 %, 2 %, 3 %, and 4 %) to investigate the effects of these materials on compaction, the resilient modulus, and the stability of electrical and electromechanical signals in cement-stabilized soil under differing degrees of saturation. Table 1 provides an overview of the properties of the MWCNTs and GNPs utilized in this study. Additionally, the morphology of both the MWCNTs and GNPs is depicted in Fig. 2.

CNMs have a considerable tendency to agglomerate, which arises from their high surface energy and the presence of strong van der Waals forces. Consequently, MWCNTs exhibit entanglement, while GNPs display overlap, as depicted in Fig. 2. To address this issue, MWCNTs/GNPs were dispersed using Pluronic F-127, a nonionic surfactant, the efficacy of which for CNM dispersion has been demonstrated in prior research studies [31,32]. However, one drawback of Pluronic F-127 is its tendency to cause excessive foaming when it is added to water due to reduced surface tension. To mitigate this challenge, tributyl phosphate 97 % (TBP 97 %), a commonly utilized plasticizer, was also employed.

Specimens preparation

The fabrication process of self-sensing cement stabilization comprises two main steps. Initially, the surfactant (Pluronic F-127) and plasticizer (TBP 97 %) were dissolved in water, and the water content was adjusted to match the desired OMC, which varied depending on the concentration of MWCNTs/ GNPs. Following the dissolution of surfactant and plasticizer, the requisite MWCNTs/GNPs were incorporated into the solution to form an aqueous solution. Notably, the dilution of the aqueous solution decreased with increasing concentrations of MWCNTs/GNPs despite the increase in OMC. Subsequently, the dry mixing of sand and 10 % cement by weight of dry sand was conducted. Once the desired quantity of dry sand with 10 % cement was thoroughly mixed, the solution prepared in the initial step was blended with the dry sand and cement mixture. All components were homogeneously mixed using varying speeds in a mixer, with manual mixing using a metal scraper performed after each time the mixer was stopped to enhance homogeneity. Upon achieving a uniformly mixed material, specimens of self-sensing cementitious composites were prepared at the $(\rho_d)_{max}$, which varied depending on the concentration of MWCNTs/GNPs. Generally, the $(\rho_d)_{max}$ decreased with increasing concentrations of MWCNTs/GNPs, while the OMC increased. Fig. 3a shows the variations in the $(\rho_d)_{max}$ and OMC based on the MWCNTs/GNPs concentration. Copper electrodes were embedded into the specimens during fabrication for electrical resistance recording; four-probe techniques were employed to minimize polarization effects resulting from electrode contact. The specimens were prepared in cubic shapes measuring 10 cm x 10 cm x 10 cm and cured for 28-days before testing, as schematically seen in Fig. 3b.

Testing methods

To assess the impact of MWCNTs/GNPs on the compaction of 10 % cement-stabilized sand, the standard Proctor test was conducted. A uniaxial compressive monotonic experiment was conducted to assess the

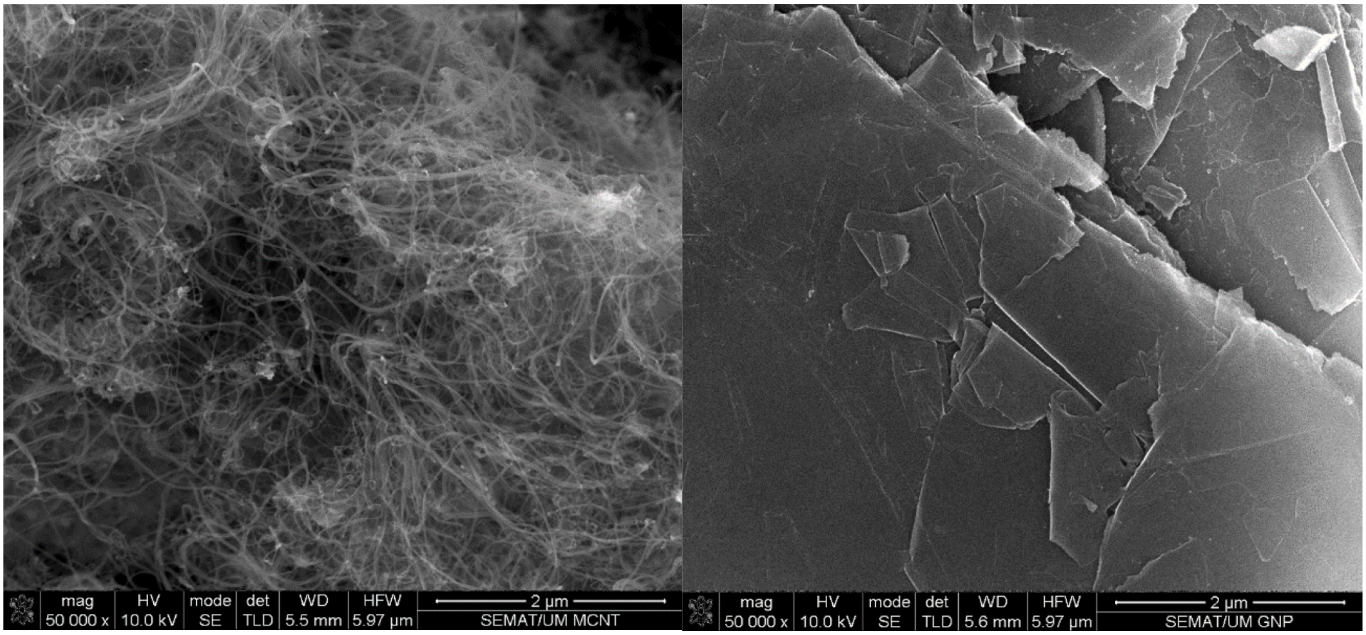
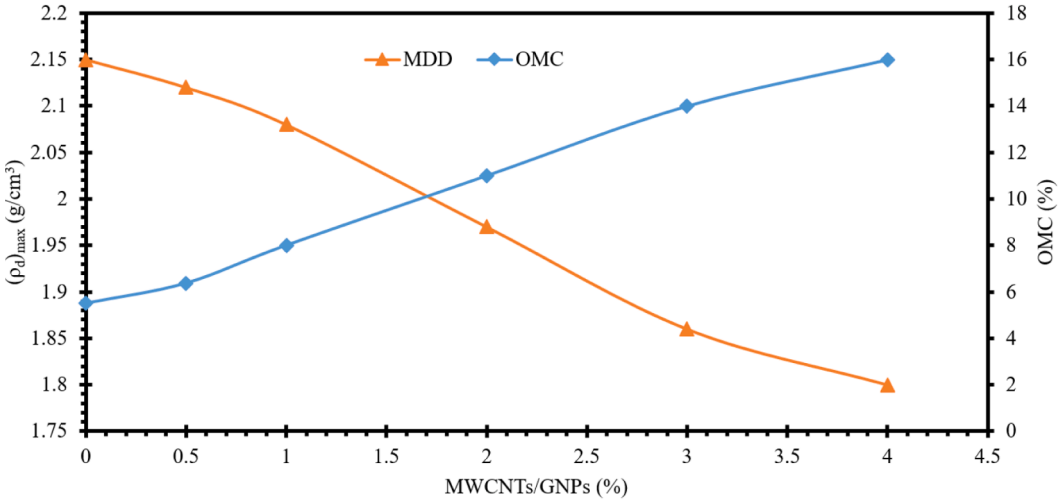
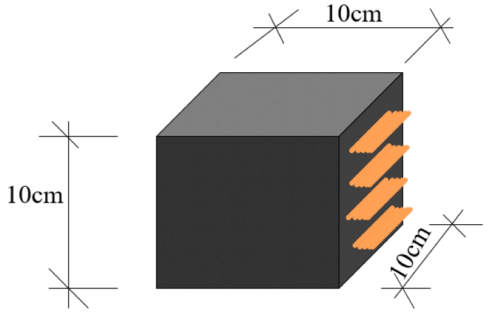


Fig. 2. Morphology of: (a) MWCNTs, and (b) GNPs.

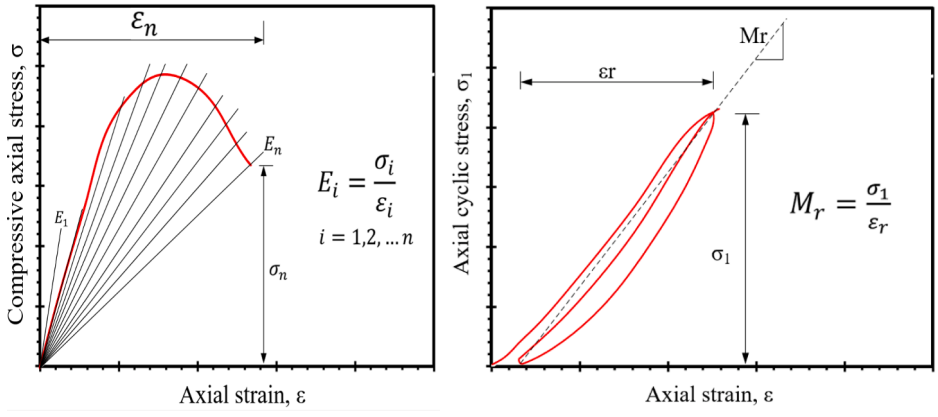


(a)



(b)

Fig. 3. (a) Variation of $(\rho_d)_{max}$ and OMC vs. MWCNT/GNP concentrations, and (b) dimension of specimens with electrodes for four-probe techniques.



(a) (b)

Fig. 4. (a) Determination of secant deformability modulus, and (b) determination of resilient modulus.

secant deformability modulus derived from the UCS, as shown in Fig. 4a. Simultaneously, electrical resistance was monitored during monotonic loading to facilitate the computation of the fractional changes in resistivity/ resistance (FCR). Furthermore, a cyclic compressive loading test was carried out to examine the influence of MWCNTs/GNPs and strain levels on the resilient modulus of 10 % cement-stabilized sand cured for 28 days. The resilient modulus was determined through analysis of the cyclic compressive loading data, as illustrated schematically in Fig. 4b.

Additionally, the effects of MWCNTs/GNPs on the electrical

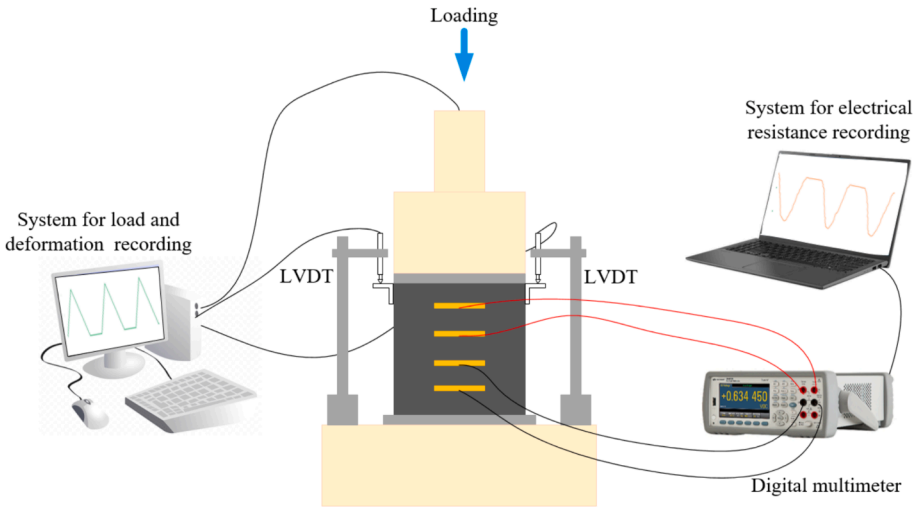
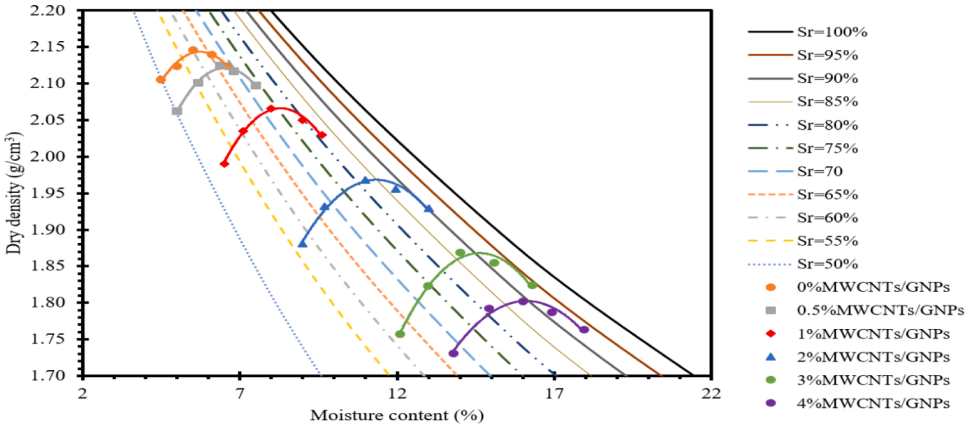
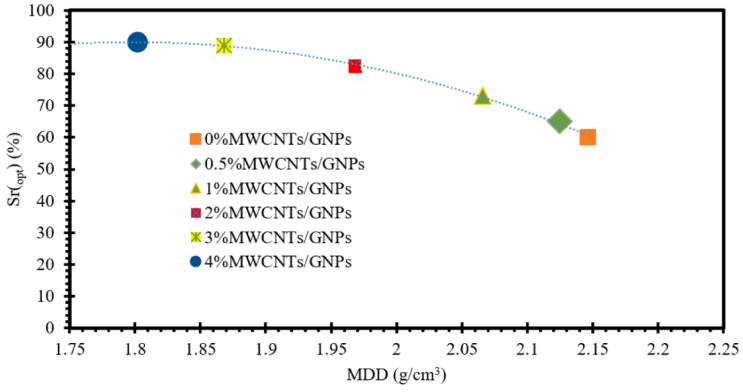


Fig. 5. Electromechanical testing setup.

resistance and piezoresistivity of 10 % cement-stabilized sand were investigated utilizing an impedance analyser known as MultiPalmSens4 and an electromechanical testing setup. To assess the stability of electrical resistance signals against variations in moisture content, the specimens were saturated to various degrees before recording the electrical resistance using MultiPalmSens4. Following an analysis of the percolation threshold and the stability of electrical resistance signals of specimens doped with various concentrations of MWCNTs/GNPs, specific specimens prepared with the minimum threshold (1 % MWCNTs/GNPs) and the maximum/optimum threshold (3 % MWCNTs/GNPs)



(a)



(b)

Fig. 6. (a) compaction curves of 10% cement stabilized soil doped with various mwcnts/gnps, (b) $(sr)_{opt}$- $(\rho_d)_{max}$ relationship for 10% cement-stabilized sand with various MWCNT/GNP %.

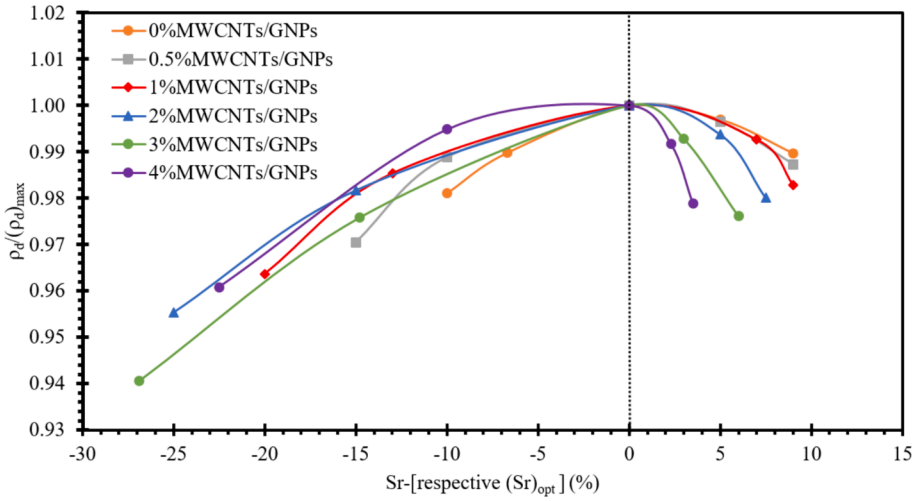


Fig. 7. Unified compaction curves of 10% cement stabilized soil doped with various MWCNTs/GNPs; $\rho_d/(\rho_d)_{max}$ vs. Sr-[respective $(Sr)_{opt}$].

were fabricated for piezoresistivity performance evaluation. In the electromechanical testing, the electrical resistance of self-sensing cement-stabilized specimens was monitored under loading conditions using a digital multimeter, as illustrated in Fig. 5. Furthermore, to further explore the effects of MWCNTs/GNPs on the 10 % cement-stabilized sand, a microcamera (Veho VMS-004 Discovery Deluxe) and SEM-FEG, Nano SEM NOVA 200, FEI were utilized.

Although the electrical resistance during the electromechanical testing was directly recorded through a digital multimeter, the principles of electrical resistance and resistivity are discussed below for reader reference. Ohm's law is used to calculate the electrical resistance, as shown in Equation (1). However, it should be noted that in the current study, the electrical resistance (R) under loading was directly recorded by a digital multimeter.

$$R = \frac{V}{I} \tag{1}$$

where R, V, and I are the electrical resistance, voltage, and electrical current, respectively.

The collected resistance was then used to calculate the electrical resistivity (ρ) based on Equation (2).

$$\rho = \frac{RA}{L} \tag{2}$$

where ρ, A, and L are electrical resistivity, cross-section area, and distance between electrodes.

After calculating the electrical resistivity, the FCR were calculated based on Equation (3) to explore the piezoresistive performance of self-sensing cement stabilized sand.

$$FCR = \frac{\Delta R}{R} = \frac{\Delta \rho}{\rho} \tag{3}$$

where ΔR is the changes in resistance, is the initial resistance, $\Delta\rho$ is the changes in resistivity, and ρ is the initial resistivity.

Equation (4) is used to evaluate the stress sensitivity (S) of self-sensing cement-stabilized sand, which is important for traffic detection and speed measurement purposes.

$$S = \frac{\Delta\rho/\rho^{*}100}{\sigma}, \%/kPa \tag{4}$$

where $\Delta\rho/\rho$ is FCR value, and σ is the stress.

The gauge factor (G) can be calculated using Equation (5). It should be noted that the G of the metallic sensor can be directly related to the Poisson ratio (ν), because the resistivity is very small compared to the strain ($\Delta\rho/\rho << \Delta L/L$); hence, Equation (5) changes to Equation (6) for the calculation of the G. On the other hand, for the G of semiconductor materials such as self-sensing cementitious composites where the resistivity variation is much larger than the strain ($\Delta\rho/\rho >> \Delta L/L$), Equation (5) changes to Equation (7) for calculation of the G. Therefore, the strain sensitivity or G of self-sensing cement-stabilized sand was computed using Equation (7).

$$G = \frac{\Delta\rho/\rho}{\Delta L/L} + 1 + 2\nu \tag{5}$$

$$G = 1 + 2\nu \tag{6}$$

$$G = \frac{FCR}{\varepsilon} = \frac{\Delta R/R}{\Delta L/L} = \frac{\Delta\rho/\rho}{\Delta L/L} \tag{7}$$

Where ν is Poisson's ratio, and ε is strain.

Results and discussion

Geotechnical characteristics

Compaction

Fig. 6 presents the compaction properties, including moisture-density relationships, for 10 % cement-stabilized sand and 10 % cement-stabilized sand with varying concentrations of MWCNTs/ GNPs (0.5 %, 1 %, 2 %, 3 %, and 4 %), as determined by the standard Proctor test. As depicted in Fig. 6, it is evident that the $(\rho_d)_{max}$ decreases as the concentration of MWCNTs/GNPs increases, while the OMC increases with increasing concentrations of MWCNTs/GNPs. The incorporation of MWCNTs/GNPs into cement-stabilized sand hinders the cement hydration reaction, thus leading to a reduction in $(\rho_d)_{max}$ probably due to formed micro voids and pores. Conversely, MWCNTs/GNPs absorb water due to their large surface area, reducing the mechanical strength of the host material [33]. Consequently, OMC increases and $(\rho_d)_{max}$ decreases with a higher percentage of MWCNTs/GNPs. This observation aligns with previous studies indicating that a lower fine content enhances compaction, whereas excessive addition of fine materials reduces the $(\rho_d)_{max}$ [34]. In previous research, an increase in the $(\rho_d)_{max}$ and mechanical strength was reported with the addition of CNMs to stabilize soils; the focus of the study was solely on the mechanical properties of soils [35]. However, in this study, higher levels of CNMs (i.e., MWCNTs/GNPs) were integrated into 10 % cement-stabilized sand to investigate not only structural properties (mechanical features) but also nonstructural properties (electromechanical properties) to create an autonomous self-sensing cement-stabilized sand. The excess incorporation of

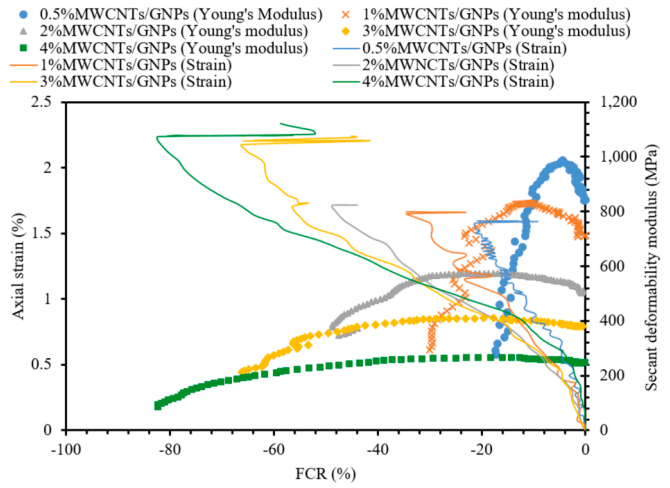


Fig. 8. Secant deformability modulus vs. FCR of self-sensing cement-stabilized sand doped with various MWCNTs/GNPs%, cured for 28-days.

MWCNTs/GNPs resulted in decreased $(\rho_d)_{max}$ and increased OMC, as indicated in Fig. 6. Nevertheless, it is worth noting that the obtained values of $(\rho_d)_{max}$ and OMC still fall within the typical ranges used for compacting transportation construction layers. Consequently, the developed self-sensing cement-stabilized sand not only possesses mechanical strength compliant with transportation standards but can also function as an autonomous self-sensing sensor to monitor stress, strain, and damage. For instance, the developed self-sensing cement stabilized sand can be utilized for the continuous monitoring of compaction quality during layer construction. In summary, the relationship between the degree of saturation at the Optimum Moisture Content (Sr)opt and maximum dry density $(\rho_d)_{max}$ presented in Fig. 6b for 10 % cement-stabilized sand doped with various concentrations of MWCNTs/GNPs is consistent with the correlation reported in a prior study, wherein the $(\rho_d)_{max}$ exhibited a decreasing trend with increasing $(Sr)_{opt}$ [36].

Monitoring soil compaction by controlling density and moisture content under a specific energy level (CEL) based on Proctor's compaction method may yield inaccurate results due to potential discrepancies between the field's CEL and that used in laboratory compaction tests. Consequently, soil stiffness control is deemed more pertinent to density and the degree of saturation rather than density and moisture content [18]. The unified compaction curve, proposed by Tatsuoka and Gomes Correia (2018) [36], offers a valuable tool for evaluating geomaterial compaction. Fig. 7 depicts the unified compaction curve for 10 % cement-stabilized sand doped with various percentages of MWCNTs/GNPs. In these findings, plotted using normalized dry density $(\rho_d/(\rho_d)_{max})$ on the vertical axis and Sr-[respective $(Sr)_{opt}$] on the horizontal axis, a common Gs value of 2.67 is assumed. The unified curves presented in Fig. 7 are consistent with those in prior reports [36]. Notably, variations in the respective $(Sr)_{opt}$ values of 10 % cement-stabilized sand with different MWCNTs/GNPs concentrations significantly altered the behaviour of self-sensing cement-stabilized sand. While the unified compaction curves exhibit similarity, a distinct trend is evident primarily on the right side, with no singular variation on the left side. At specific Sr-[respective $(Sr)_{opt}$] values on the right side of Fig. 7, the normalized $\rho_d/(\rho_d)_{max}$ value of 10 % cement-stabilized sand decreases with increasing MWCNT/GNP concentration, indicating effective dispersion of MWCNTs/GNPs due to excessive water content. Conversely, the lack of a unique trend on the left side of the curves is attributed to agglomeration resulting from the weak dispersion of the carbon nanomaterials. Consequently, to achieve the desired compaction level in the field, the Sr level must reach $(Sr)_{opt}$, leading to a dry density (ρ_d) that ensures the desired mechanical strength [36].

Secant deformability modulus

It is imperative to comprehend the deformability of soils across a spectrum ranging from very small strains to failure [37]. In this regard, the correlation between the secant deformability modulus and FCR of 10 % cement-stabilized-sand containing various percentages of MWCNTs/GNPs is depicted in Fig. 8. This figure elucidates key insights regarding self-sensing cementitious geocomposites. First, it is evident that the stiffness of the cement-stabilized sand decreases with an increase in the percentage of MWCNTs/GNPs. This reduction in stiffness is ascribed to the attenuation of cementation bonding, stemming from delayed or impeded hydration processes caused by excess carbon nanotube materials.

Second, Fig. 8 indicates that the FCR increases proportionally to the increase in the percentage of MWCNTs/GNPs, suggesting enhanced sensitivity. Additionally, the secant deformability modulus demonstrates either an increase or a constant trend with respect to FCR up to a certain threshold. This region of consistent or increasing deformability modulus signifies structural integrity, which is denoted as the elastic or quasi-elastic region. Conversely, beyond this threshold, where the deformability modulus decreases with increasing FCR, the onset of cement-stabilized sand degradation occurs. Notably, greater decreases in the deformability modulus correspond to cracks. For instance, the secant deformability modulus of cement-stabilized sand doped with 0.5 % and 1 % MWCNTs/GNPs exhibited a drastic reduction after a certain

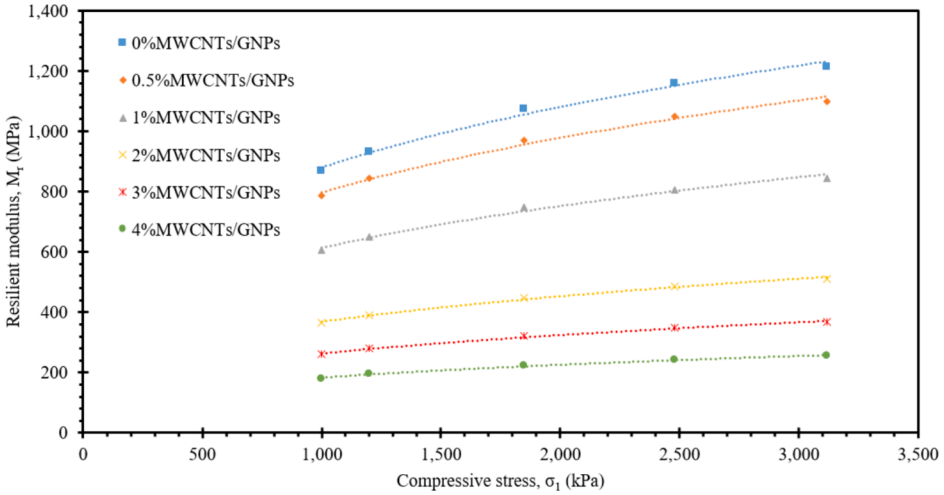


Fig. 9. Resilient modulus vs. compressive loading within quasi-elastic region for 10% cement-stabilized sand doped with various MWCNTs/GNPs, cured for 28-days.

threshold, indicating the occurrence of cracks due to their enhanced brittleness.

Furthermore, the fluctuation of FCR in Fig. 8 correlates with the crack conditions under compressive monotonic loading. As the crack size diminishes during compressive monotonic loading, the FCR decreases, while an increase in the crack dimensions leads to a rise in the FCR. Unlike in compressive cyclic loading, in which the FCR fluctuates with loading and unloading cycles, the FCR generally increases with respect to the deformability modulus under compressive monotonic loading. Regarding Fig. 8, it is evident that the FCR increases proportionally to the increase in percentage of MWCNTs/GNPs. This correlation stems from the enhanced ductility observed in 10 % cement-stabilized sand incorporating MWCNTs/GNPs. This inference is supported by the axial strain levels, which demonstrate a concurrent increase with the MWCNTs/GNPs percentage. Put differently, the increase of concentration of MWCNTs/GNPs leads to the decrease in the secant deformability modulus and the increase in the FCR, attributed to the enhanced ductility, as corroborated by the axial strain data presented in Fig. 8. The continual assessment of the stiffness of cement stabilized soil holds paramount importance [38]. In this context, the correlation between FCR and Secant deformability modulus can thus be utilized for the continual evaluation of the stiffness of cement stabilized sand.

Resilient modulus

Fig. 9 shows the resilient modulus (Mr) as a function of the compressive stress (within the elastic region) of 10 % cement-stabilized sand with various concentrations of MWCNTs/ GNPs cured for 28-days. Fig. 9 shows that the resilient modulus increases with increasing compressive stress. This finding aligns with prior research indicating that the resilient modulus of granular soils, including sand and unbound granular materials (UGM), tends to increase with increasing axial stress [39]. In UGM materials, this increase in Mr with increasing axial stress is attributed to stress-hardening behaviour, while in cement-stabilized sand, is primarily driven by the progressive development of cementitious bonds, improved stress transfer mechanisms, particle packing, and strain hardening effects. These factors collectively contribute to the material's ability to withstand higher loads and exhibit greater stiffness under applied stress conditions. Nevertheless, beyond a certain threshold, that can be defined quasi-elastic threshold, the resilient modulus of cement-stabilized soil under compressive loading may decrease due to the degradation of material bonding induced by cyclic loading and strain accumulation [40]. However, in this section, the focus was on investigating the behavior within the quasi-elastic region by applying cyclic compressive loading, as depicted in Fig. 9. Additionally, the variation in the Mr of cement-stabilized soil is contingent upon the rigidity of the soil, wherein the resilient modulus of cement-stabilized soil with lower UCS values tends to decrease with compressive cyclic loading, while the resilient modulus of soil with higher UCS values (>690 kPa) increases with increasing cyclic compressive loading [41]. Accordingly, the Mr of 10 % cement stabilized-soil doped with various concentrations of MWCNTs/GNPs increases with increasing cyclic compressive stress, potentially owing to its increased stiffness.

With reference to Fig. 9, it becomes apparent that the rate of increase in Mr with an increase in cyclic compressive stress is contingent upon the concentration of MWCNTs/GNPs. Specifically, the rate of increase in Mr decreases with increasing concentrations of MWCNTs/GNPs due to reduced stiffness (as evidenced by the decrease in the slope of the lines in Fig. 9 with increasing MWCNT/GNP concentrations). In essence, the introduction of MWCNTs/GNPs into 10 % cement-stabilized sand hinders cement hydration, diminishing the stiffness, and integrity of the material. As a result, the rate of increase in the resilient modulus in response to cyclic compressive loading decreases with increasing concentrations of MWCNTs/GNPs.

Various models have been utilized to establish a relationship between the obtained resilient modulus of granular soils and compressive cyclic loading [42]. Among these models, the power law model described in Equation (9) has attracted attention for its simplicity; it requires only two parameters: K_1 and K_2. Therefore, in this study, the power law model was employed to examine the laboratory data, and is aligned with previous research findings showing that the vertical elastic Young's modulus was essentially a unique function of the vertical (axial) stress, while it was rather independent of the horizontal (lateral) stress [43]. The values of these parameters, as outlined in Table 2, were derived through regression analysis of the laboratory data.

Table 2
Regression coefficients.

CNMs	K_1	K_2	R^2
0	114.05	0.2958	0.99
0.5	103.53	0.2954	0.99
1	79.636	0.2954	0.99
2	46.937	0.2983	0.99
3	32.639	0.3021	0.99
4	23.011	0.3004	0.98

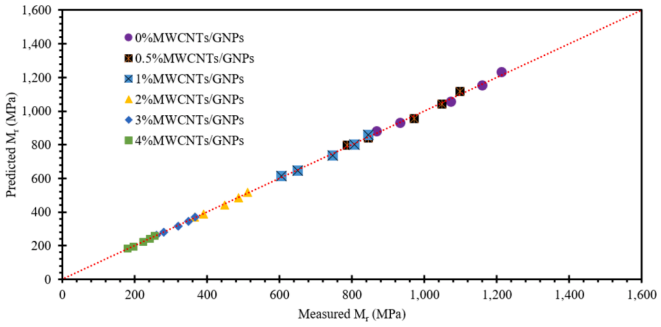


Fig. 10. Predicted vs. measured resilient modulus of cement-stabilized sand with various MWCNT/GNP %, cured for 28-days.

$$M_r = K_1 \times \sigma_1^{K_2} \quad (9)$$

The adjustment between the experimentally determined resilient modulus from laboratory data and the predicted resilient modulus obtained through the power law model is depicted in Fig. 10. This figure highlights a substantial fit between the measured and predicted resilient moduli, underscoring the credibility of the experimental data and the efficacy of the predictive model.

To thoroughly assess the impact of MWCNTs/GNPs on the resilient modulus of 10 % cement-stabilized sand, the correlation depicted in Fig. 11 must be examined. Fig. 11 clearly shows that the resilient modulus decreases with increasing MWCNT/GNP concentration under various compressive stresses. This trend mirrors similar findings reported in prior research, where an increase in MWCNT concentration led to a decrease in compressive strength [44]. Previous studies have generally indicated that the inclusion of very small amounts of CNTs can enhance the strength of cementitious composites due to nucleation effects that augment cement hydration [45]. However, the excessive amounts of CNTs into cementitious composites has been shown to decrease mechanical strength of the composites due to the hydration reaction inhibition caused by the surface coating of cement particles and the high potential for agglomeration [46]. Achieving increased mechanical strength and desirable electromechanical properties in cementitious composites upon increasing the incorporation of carbon nanomaterials is indeed challenging. While incorporating very small amounts of carbon nanomaterials into the composites may enhance mechanical strength, it has been reported in prior studies that it is impractical to achieve nonstructural properties (such as electromechanical performance) in cement-stabilized sand by incorporating MWCNTs/GNPs at concentrations lower than 0.5 % or even 1 % [8]. Thus, in the present study, higher concentrations of MWCNTs/GNPs

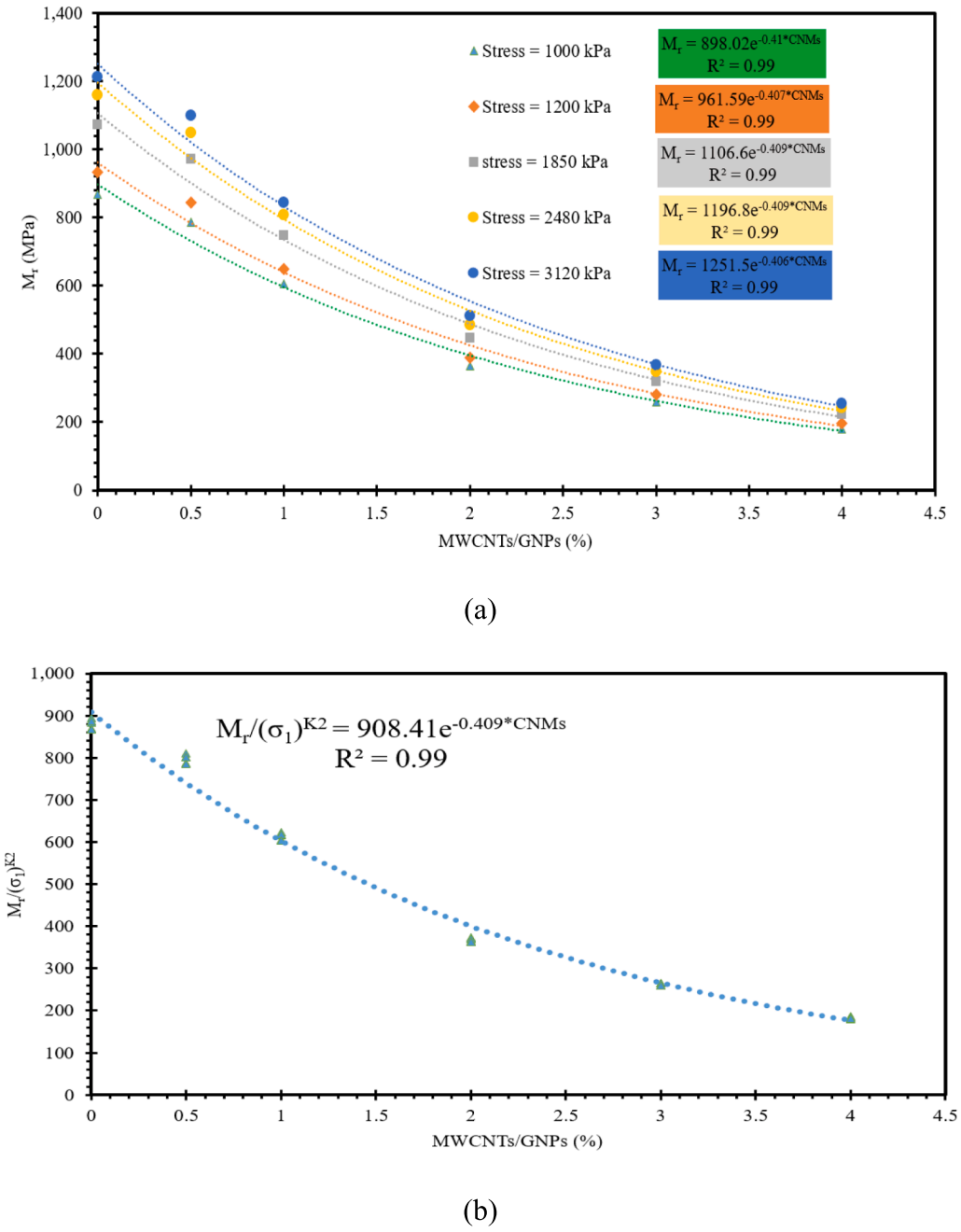
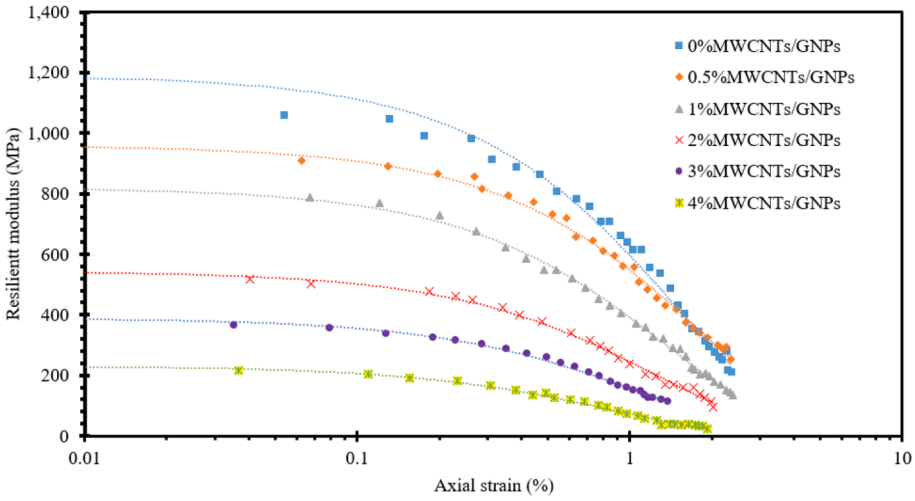


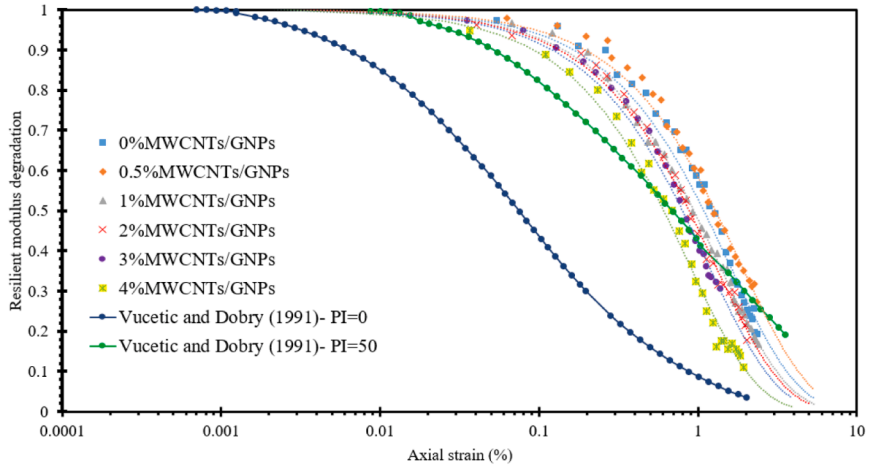
Fig. 11. (a) Resilient modulus (MPa) vs. MWCNT/GNP (%) under various compressive stresses of specimens cured for 28-days, and (b) normalized resilient modulus vs. MWCNT/GNP %, cured for 28-days.

were integrated into cement-stabilized sand to keep the resilient modulus within the range of materials typically utilized in transportation construction layers and to enhance the electromechanical performance of the geocomposite for autonomous self-sensing purposes. Despite the decrease in the resilient modulus with increasing MWCNT/GNP concentration, the resilient modulus values depicted in Fig. 11 align with the typical values of geomaterials used in transportation construction layers [47]. An unique relationship was obtained between the normalized resilient modulus against stress ($M_r/(\sigma_1)^{K2}$) and the MWCNT/GNP concentration as shown in Fig. 11b.

The resilient modulus with respect to the developed axial strain is presented in Fig. 12a. The significance of the nonlinear correlation between resilient modulus and strain depicted in Fig. 12a is crucial for the design of railway tracks [48]. Fig. 12a, clearly shows that the decrease in the resilient modulus of both plain cement-stabilized sand and cement-stabilized sand containing MWCNTs/GNPs increases with increasing strain levels. The introduction of strain damages the interparticle bonds within the cement-stabilized soil, leading to a reduction in the resilient modulus. These results are consistent with prior research in which a decrease in the resilient modulus of geomaterials was reported with increasing strain [49,50]. The resilient modulus degradation of 10 % cement-stabilized sand ($Mr/Mr_{(max)}$) doped with various amounts of MWCNTs/GNPs was compared with the degradation curves of cohesionless and cohesive soils from previous studies [50], and the degradation curves are presented in Fig. 12b. A comparison of the findings in Fig. 12b indicates that the resilient modulus degradation at smaller strain levels is relatively insignificant for 10 % cement-stabilized sand and with a quasi-elastic strain threshold higher for the natural soils. However, beyond a certain strain threshold, the rate of decrease in resilient modulus degradation notably accelerates. This phenomenon



(a)



(b)

Fig. 12. (a) resilient modulus of 10% cement-stabilized sand doped with various mwcnts/gnps vs. axial strain, cured for 28-days, and (b) comparison of resilient modulus degradation curves of natural soils with plasticity index (pi) ranging from 0 to 50 [50] with that of 10% cement-stabilized sand doped with various MWCNTs/GNPs %, cured for 28-days.

can be attributed to the strain-softening behavior observed in cement-stabilized soils, in which a sudden decrease of stiffness occurs after the initiation of micro cracks and plastic deformations [22]. Furthermore, the increasing rate of resilient modulus degradation with increasing strain levels can also be linked to the absence of confining pressure in the testing setup. In cases where confining pressure is applied, the degradation rate of resilient modulus in stabilized sand exhibits a gradual decreasing trend with increasing strain, possibly due to the mitigation or prevention of strain-softening behaviour [51]. Essentially, the confining pressure limits both lateral and axial deformation, reducing resilient modulus degradation. Fig. 12b shows that the resilient modulus degradation in cement-stabilized sand increases with increasing concentrations of MWCNTs/GNPs. For instance, at a shear strain of 0.3 %, the normalized resilient modulus of 10 % cement-stabilized sand decreased from 0.83 for plain cement-stabilized sand to 0.72 for cement-stabilized sand doped with 4 % MWCNTs/GNPs. The accelerated rate of degradation observed in cement-stabilized sand with increasing concentrations of MWCNTs/GNPs at a constant strain can be attributed to the weakening of interparticle bonding forces. As previously discussed, excessively high concentrations of MWCNTs/GNPs lead to a reduction in cementation bonding facilitated by cement hydration, resulting in reduced stiffness of the cement-stabilized sand. However, the decrease in the resilient modulus of 10 % cement-stabilized sand containing various concentrations of MWCNTs/GNPs is less pronounced than that of untreated cohesionless and cohesive soils, as illustrated in Fig. 12b. For example, at a shear strain of 0.3 %, the normalized stiffness of 10 % cement-stabilized sand containing 4 % MWCNTs/GNPs is 0.72. In contrast, for untreated cohesionless and cohesive soils under the same shear strain (0.3 %), the normalized stiffness values are 0.23 and 0.65, respectively, as illustrated in Fig. 12b. These findings suggest that the addition of MWCNTs/GNPs to cement-stabilized sand not only improves its nonstructural properties (such as self-sensing functionality) but also enhances its mechanical strength compared to those of untreated cohesionless and cohesive soils. It is important to highlight that the strain for the degradation curve results presented in this study were derived from LVD measurements in unconfined compression tests, whereas the resilient modulus data for untreated cohesionless and cohesive soils found in the literature were obtained through triaxial tests

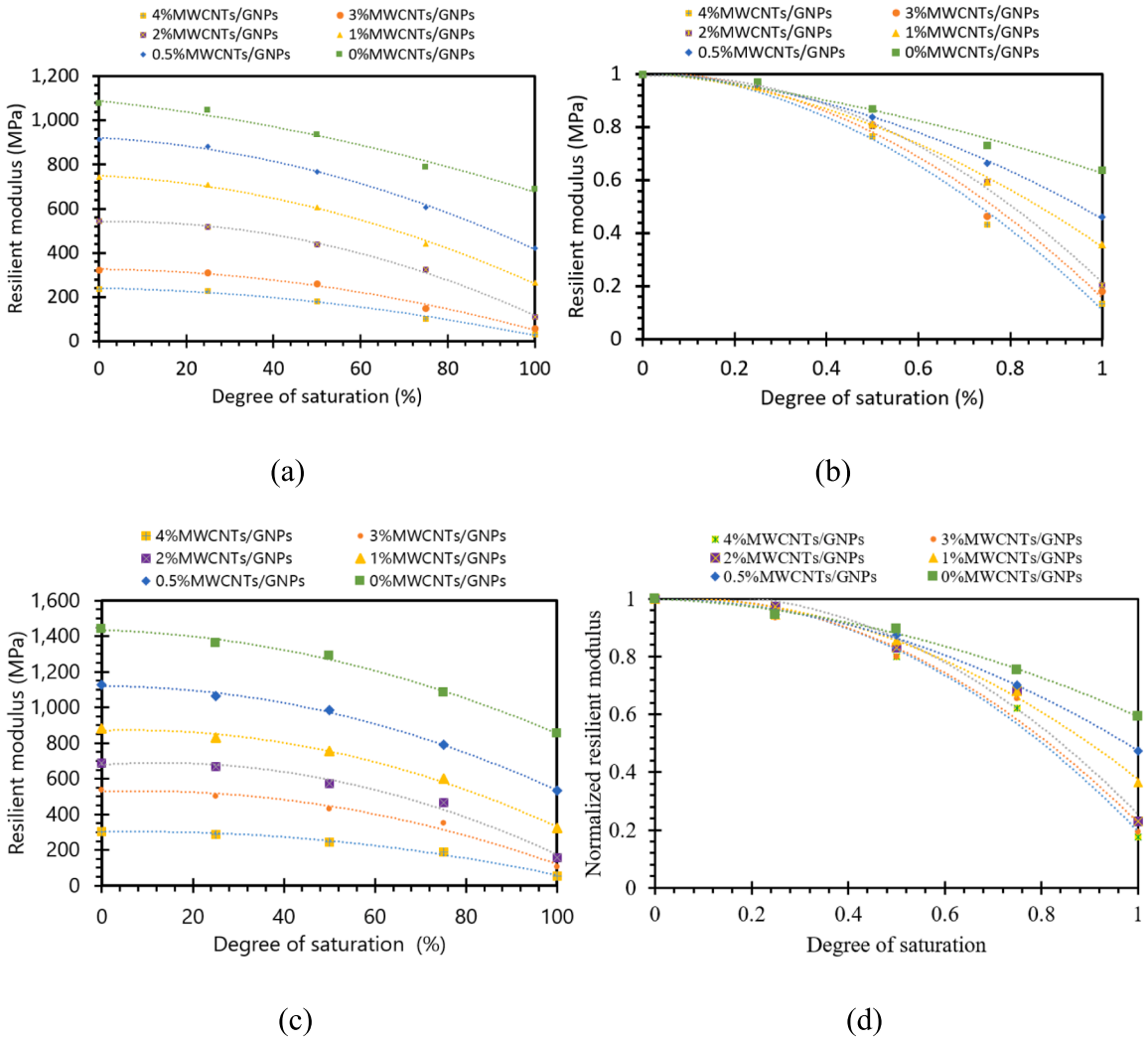


Fig. 13. Resilient modulus vs. degree of saturation for specimens cured for 28-days: (a) resilient modulus under 1000 kPa, (b) normalized resilient modulus under 1000 kPa, c) resilient modulus under 3120 kPa, and d) normalized resilient modulus under 3120 kPa.

and resonant column tests. Consequently, in future investigations, cement-stabilized sand with diverse MWCNT/GNP compositions should also be evaluated via advanced geotechnical testing equipment. In this context, the utilization of cyclic triaxial testing with localized instrumentation on the specimen can be utilized [43,52].

The resilient modulus of soils is influenced by their degree of saturation. For example, the resilient modulus of 10 % cement-stabilized sand containing different percentages of MWCNTs/GNPs, subjected to cyclic compressive loading of 1000 kPa and 3120 kPa, decreases as the degree of saturation increases, as illustrated in Fig. 13. These findings align with prior research indicating a decrease in the resilient modulus with increasing moisture content, attributed to decreasing matric suction [53]. The relationship between matric suction (u_a-u_w) and the degree of saturation (S_r) is established through a soil water characteristic curve (SWCC), in which matric suction decreases with increasing degree of saturation. Consequently, as the degree of saturation increases, matric suction decreases, resulting in a decrease in the resilient modulus [54], as evidenced in Fig. 13a and c for 10 % cement-stabilized sands containing 0 %, 0.5 %, 1 %, 2 %, 3 %, and 4 % MWCNTs/GNPs respectively under 1000 kPa and 3120 kPa. However, it is worth noting that the resilient modulus at 100 % saturation does not reach zero and remains relatively high due to the cementation bonding facilitated by cement hydration, as depicted in Fig. 13. In essence, two types of cementation bonding exist between sand particles in cement-stabilized sand: bonding originating from cement hydration and bonding arising from matric suction. Therefore, even under fully saturated conditions under which matric suction decreases due to increased degree of saturation, the cementation bonding resulting from cement hydration persists. Consequently, cement-stabilized sand maintains a significant resilient modulus even under fully saturated conditions. Nevertheless, understanding the variation in the resilient modulus with the degree of saturation or matric suction is crucial for the continuous monitoring of transportation construction layers through different seasons of the year.

Fig. 13b and d illustrate that the decrease in the resilient modulus due to an increase in the degree of saturation is more pronounced for cement-stabilized sand containing MWCNTs/GNPs. The addition of MWCNTs/GNPs to cement-stabilized sand leads to greater water absorption, likely due to weakened cementation bonding resulting from cement hydration inhibition. Consequently, at a specific degree of saturation, the rate of resilient modulus degradation increases with increasing concentrations of MWCNTs/GNPs, as depicted in Fig. 13b.

Nonstructural characteristics

Electrical percolation theory

Incorporating nonstructural characteristics and self-sensing capabilities, such as stress sensing, strain sensing, and damage detection, into cement-stabilized sand requires the addition of an appropriate

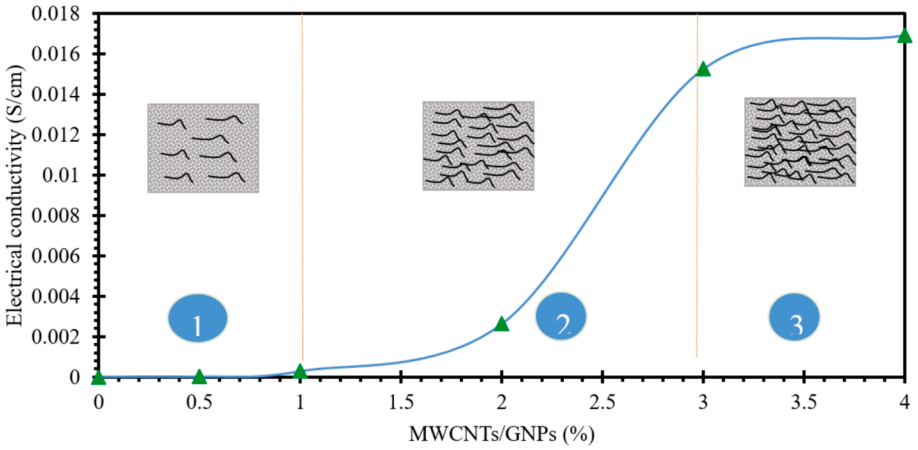
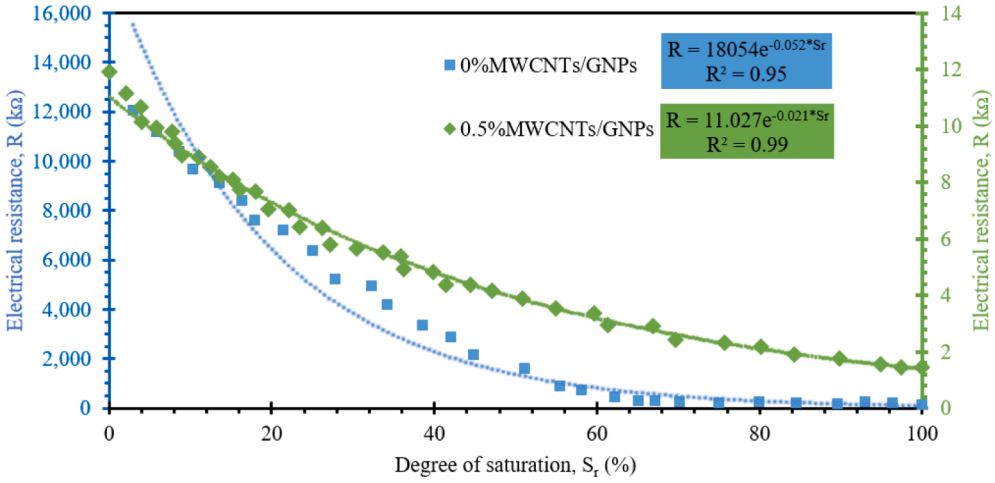
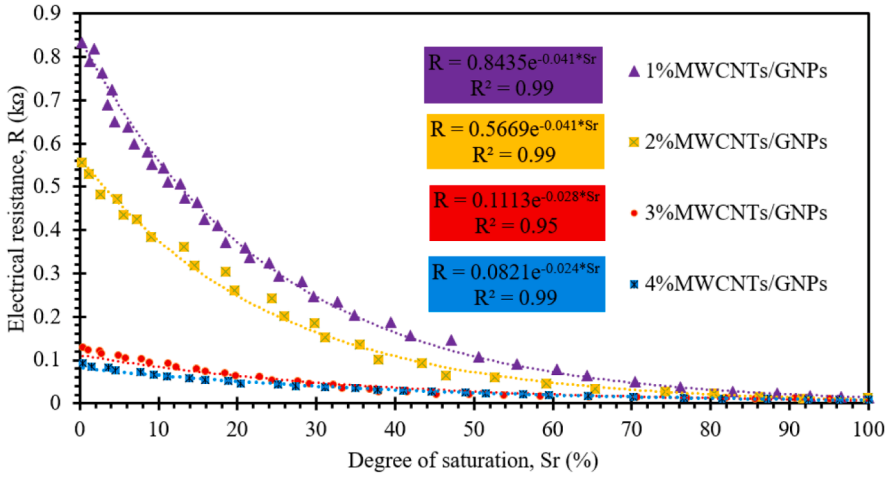


Fig. 14. Electrical conductivity with respect to MWCNT/GNP %.



(a)



(b)

Fig. 15. Electrical resistance vs. degree of saturation for specimens cured for 28-days: (a) plain specimen "10% cement-stabilized sand" and 10% cement-stabilized sand doped with 0.5% MWCNT/GNP; (b) 10% cement-stabilized sand doped with 1%, 2%, 3%, and 4% MWCNTs/GNPs.

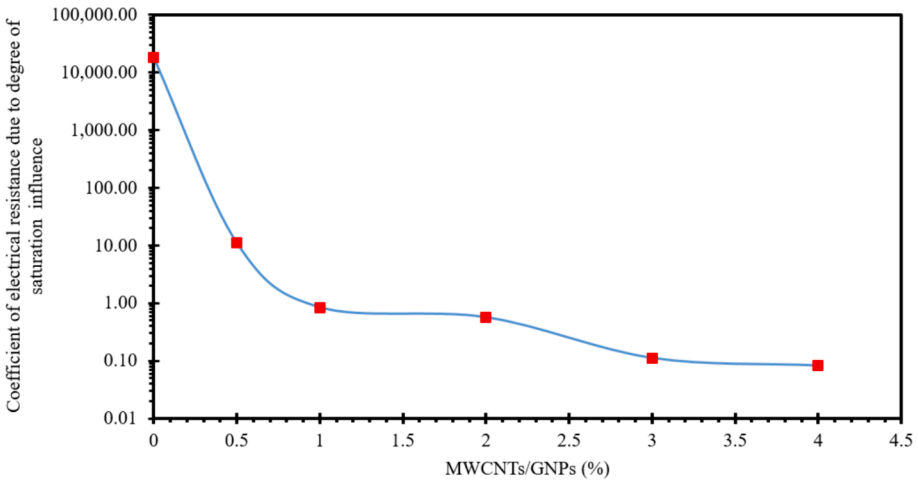


Fig. 16. The influence level of degree of saturation on cement-stabilized sand doped with various MWCNT/GNP percentages for specimens cured for 28-days.

percentage of conductive fillers. In this context, the application of electrical percolation theory plays a pivotal role in designing multifunctional cement-stabilized sand. Fig. 14 illustrates the S-shaped percolation curve of self-sensing cement-stabilized sand incorporating MWCNTs/GNPs, which illustrates three distinct regions: insulation, percolation threshold, and conductivity [55]. In the initial region (insulation), the increase in electrical conductivity of cement-stabilized sand is marginal due to the formation of poor conductive pathways resulting from the low percentage of MWCNTs/GNPs. This indicates that the concentration of conductive filler within this region is insufficient to produce multifunctional cement-stabilized sand. Although the electrical conductivity in the first region may increase with the increase of pore solution based on the ionic conductivity mechanisms, in dry conditions, the electrical conductivity of cement stabilized sand doped with MWCNTs/GNPs within the insulation region range. This results in insufficient self-sensing capabilities due to limited electron transport [56]. The second region is the percolation, where the electrical conductivity of cement-stabilized sand witnesses a significant enhancement in electrical conductivity with MWCNTs/GNPs inclusion ranging from 1 % to 3 %. Within the percolation threshold, the concentration of MWCNTs/GNPs is sufficient to form adequately conductive pathways through direct contact, tunneling effects, and ionic conduction in wet conditions, as well as direct contact and tunneling effects in dry conditions, enabling considerable electron transport [56]. In the third region (conductivity), the enhancement in electrical conductivity of cement-stabilized sand is negligible upon further inclusion of MWCNTs/GNPs beyond 3 %, as congested conductive pathways already exist. Considering the congested conductive pathways formed by an excessive percentage of MWCNTs/GNPs, the primary conductivity mechanism in the third region is based on direct contact between conductive fillers. Fig. 14 shows that to produce self-sensing cement stabilized sand with significant piezoresistive performance, the percentage of conductive filler should fall within the percolation threshold region.

Electrical resistance

The moisture content or degree of saturation significantly impacts the electrical resistivity of both plain cement-stabilized sand and cement-stabilized sand containing MWCNTs/GNPs, as illustrated in Fig. 15. Similar findings concerning the influence of moisture content on the electrical resistance of cement composites doped with CNTs have been reported in prior research [57], supporting the outcomes of the present study on self-sensing cement-stabilized sand. The effect of the degree of saturation on the electrical resistance of cement-stabilized sand varies depending on the concentration of MWCNTs/GNPs, as observed in Fig. 15a to d. Fig. 15 clearly shows that the impact of the degree of saturation on the electrical resistance diminishes as the percentage of MWCNTs/GNPs increases. Higher concentrations of MWCNTs/GNPs correspond to a lesser effect of the degree of saturation on the electrical resistance of cement-stabilized sand. These findings corroborate the electrical percolation theory discussed earlier for cement-stabilized sand. According to this theory, the reduction in the electrical conductivity of cement-stabilized sand is not significant with the inclusion up to 1 % of MWCNTs/GNPs due to inadequate electron conductive pathways. Therefore, the influence of the degree of saturation on the electrical resistance of cement-stabilized sand doped with MWCNTs/GNPs below the percolation threshold is considerable, as evidenced by the exponential equations in Fig. 15. Conversely, the influence of the degree of saturation on the electrical resistance of self-sensing cement stabilized sand doped with MWCNTs/GNPs within the percolation threshold and conductivity regions is negligible, as depicted in Fig. 15b, owing to well-established conductive pathways.

In summary, when the concentration of conductive filler falls below the percolation threshold, the influence of the degree of saturation and moisture content on the electrical resistance of cement-stabilized sand is significant due to abundant ionic conduction and lack of electron conduction. As observed in Fig. 15, the initial electrical resistance of cement-stabilized sand doped with MWCNTs/GNPs below the percolation threshold was notably high under dry conditions (0 degrees of saturation) due to inadequate electron conduction pathways. Subsequently, the electrical resistance of cement-stabilized sand containing MWCNTs/GNPs below the percolation threshold decreased significantly with increasing degree of saturation due to the ionic conduction induced by the pore solution.

Conversely, the initial electrical resistance of cement-stabilized sand doped with MWCNTs/GNPs exceeding the percolation threshold is relatively low due to existing electron conduction, as shown in Fig. 15d. Additionally, Fig. 15d shows that the influence of the degree of saturation on the electrical resistance of cement-stabilized sand doped with 2 %, 3 %, and 4 % MWCNTs/GNPs is negligible. It should be noted that a conventional DC multimeter is inadequate for measuring the electrical resistance of cement-stabilized sand containing 0 % MWCNTs/GNPs, particularly under dry conditions. Therefore, in the present study, an impedance analyser MultiPalmSens4, was employed to record the electrical resistance.

Electrical resistance tomography is an effective method for monitoring moisture variations in geomaterials in the field [58]. Consequently, the findings regarding the influence of moisture content on the electrical resistance of self-sensing cement-stabilized sand containing MWCNTs/GNPs can be valuable for calibrating electrical resistance tomography in field applications in which this self-sensing cement-stabilized sand is utilized.

To further investigate the impact of the degree of saturation on the

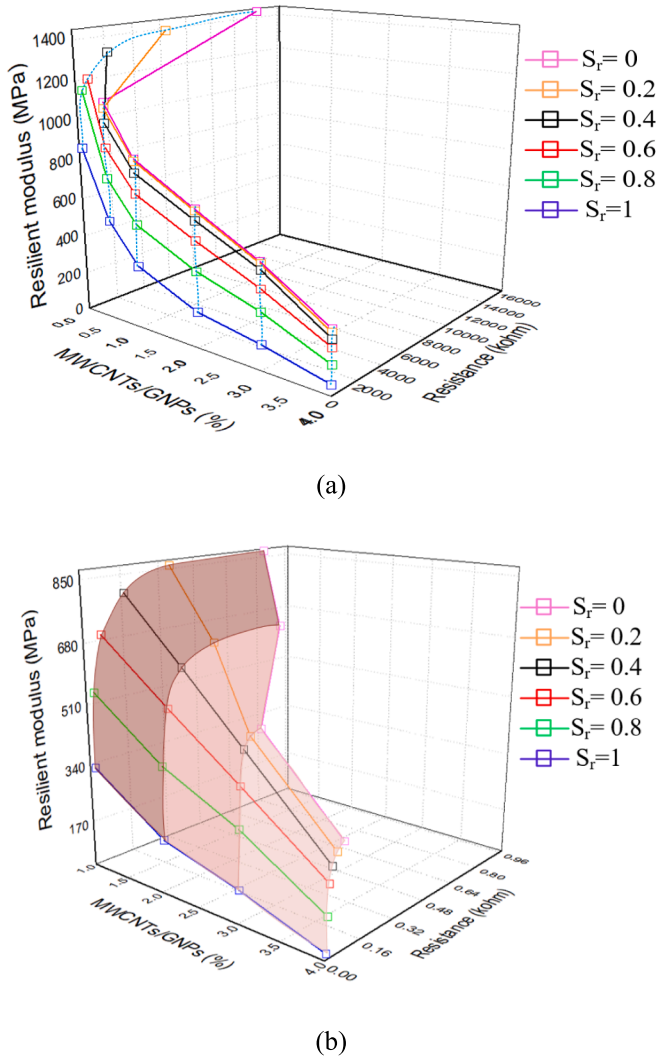


Fig. 17. Correlation between resilient modulus, and MWCNTs/GNPs % and electrical resistance under σ1 = 3120 kPa under different degrees of saturation for specimens cured for 28-days: (a) MWCNTs/GNPs ranging from 0 % to 4 %; (b) MWCNTs/GNPs ranging from 1 % to 4 %.

reduction in electrical resistance in cement-stabilized sand with various proportions of MWCNTs/GNPs, a plot was generated based on the coefficients derived from the equations provided in Fig. 15, and the results are presented in Fig. 16. Fig. 16 reveals that the reduction coefficient of electrical resistance resulting from the degree of saturation is notably greater for cement-stabilized sand doped with MWCNTs/GNPs (below 1 %) than for those doped with higher concentrations of MWCNTs/GNPs. This observation suggests that to achieve stable self-sensing cement-stabilized sand that is resistant to moisture content fluctuations, the percentage of MWCNTs/GNPs should exceed 1 % (falling within the percolation threshold). These findings represent a valuable contribution to the application of self-sensing cement-stabilized sand in real-life projects, in which fluctuations in moisture levels throughout the year can significantly impact the electromechanical performance of such materials.

The relationships between the resilient modulus, percentage of MWCNTs/GNPs, and electrical resistance across various degrees of saturation are illustrated in Fig. 17a. Fig. 17a shows a positive correlation between the resilient modulus and electrical resistance, and a negative correlation between the percentage of MWCNTs/GNPs and the degree of saturation. Specifically, as the percentage of MWCNTs/GNPs increases, there is a corresponding decrease in electrical resistance, leading to a delayed or inhibited cement hydration process and consequently a reduction in the resilient modulus. Furthermore, the resilient modulus decreases with increasing degree of saturation due to reduced matric suction and compromised cementation bonding.

To elucidate the relationship between the resilient modulus, electrical resistance, and percentage of MWCNTs/GNPs, Fig. 17a was replotted specifically for cement-stabilized sand containing MWCNT/GNP concentrations ranging from 1 % to 4 %, as depicted in Fig. 17b. Fig. 17b shows that the resilient modulus decreases with increasing percentages of MWCNTs/GNPs, increasing degrees of saturation, and decreasing electrical resistance.

The insights provided regarding electrical resistance in this study can be utilized to establish a correlation between the mechanical strength and electrical signals in cement-stabilized sand with different proportions of MWCNTs/GNPs. Fig. 18 illustrates the correlation between the electrical resistance and resilient modulus of cement-stabilized sand doped with varying concentrations of MWCNTs/GNPs under $\sigma_1 = 3120$ kPa under dry conditions/zero degrees of saturation. Fig. 18 clear shows that the resilient modulus decreases as the electrical resistance decreases. This observation is consistent with findings from previous studies on geomaterials using geophysical data, in which it was observed that the shear strength of soil decreased as electrical conductivity increased [59].

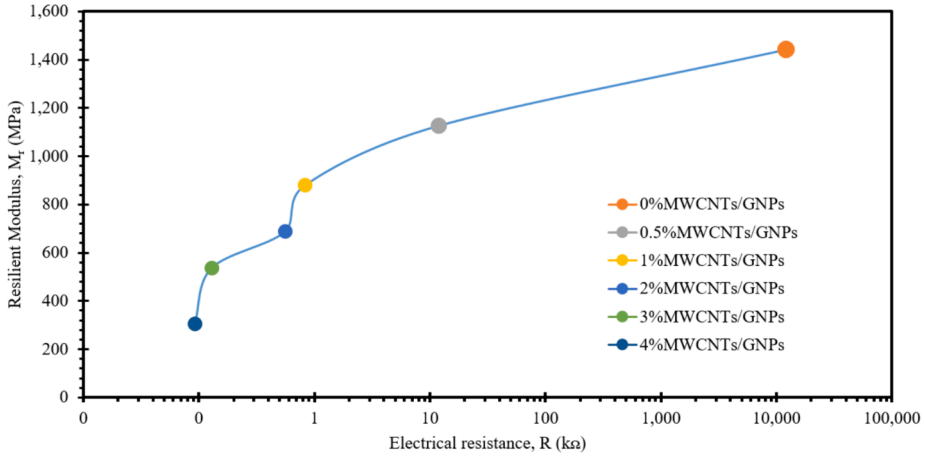
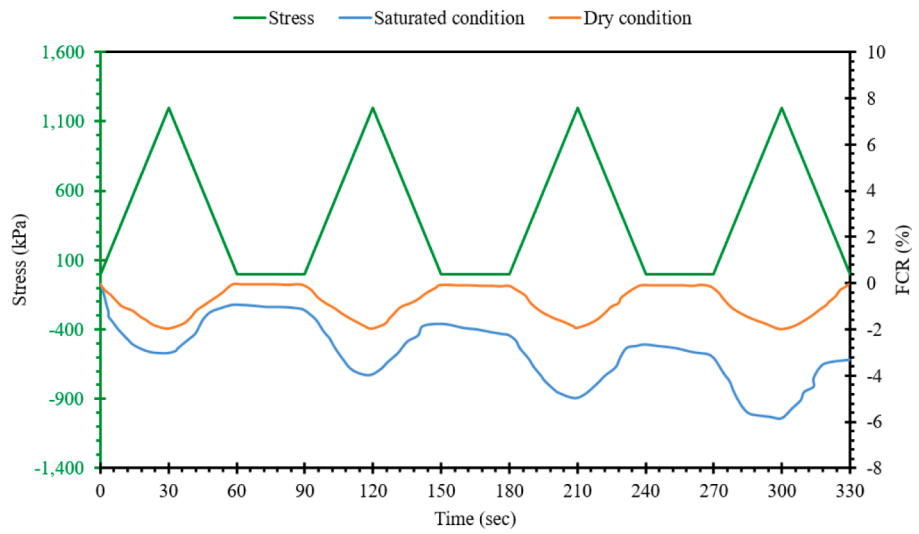
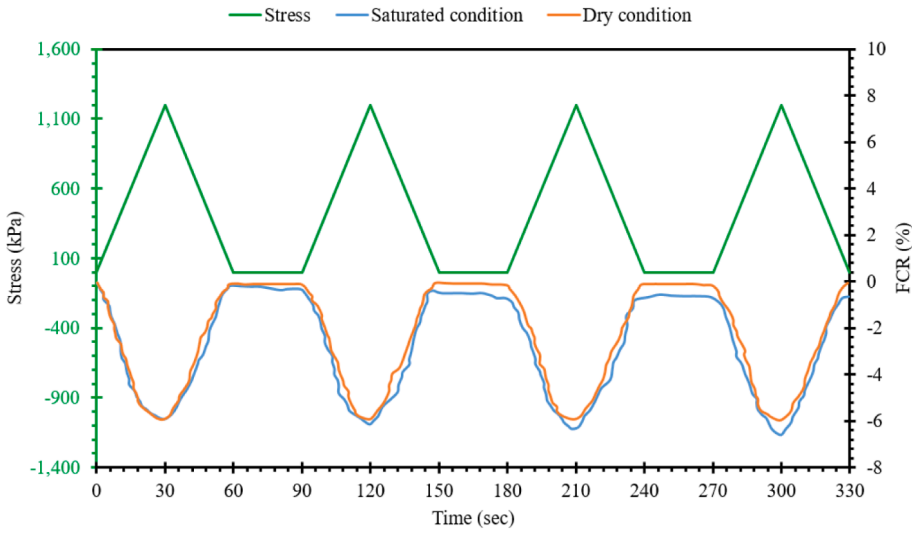


Fig. 18. Correlation between the electrical resistance and resilient modulus under $\sigma_1 = 3120$ kPa at dry conditions/zero degrees of saturation for specimens cured for 28-days.



(a)

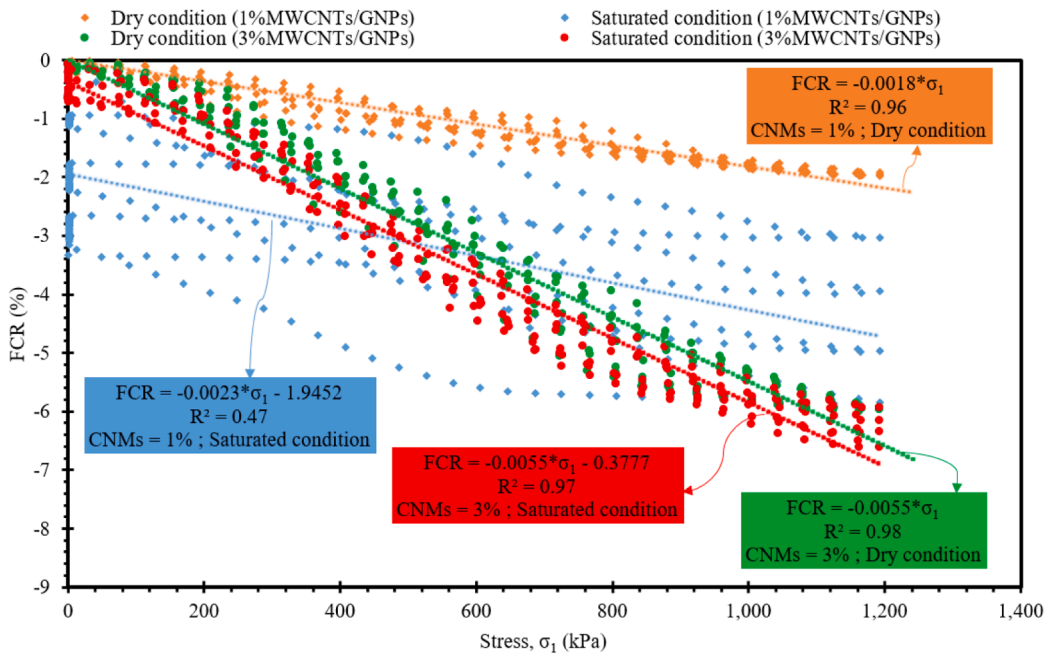


(b)

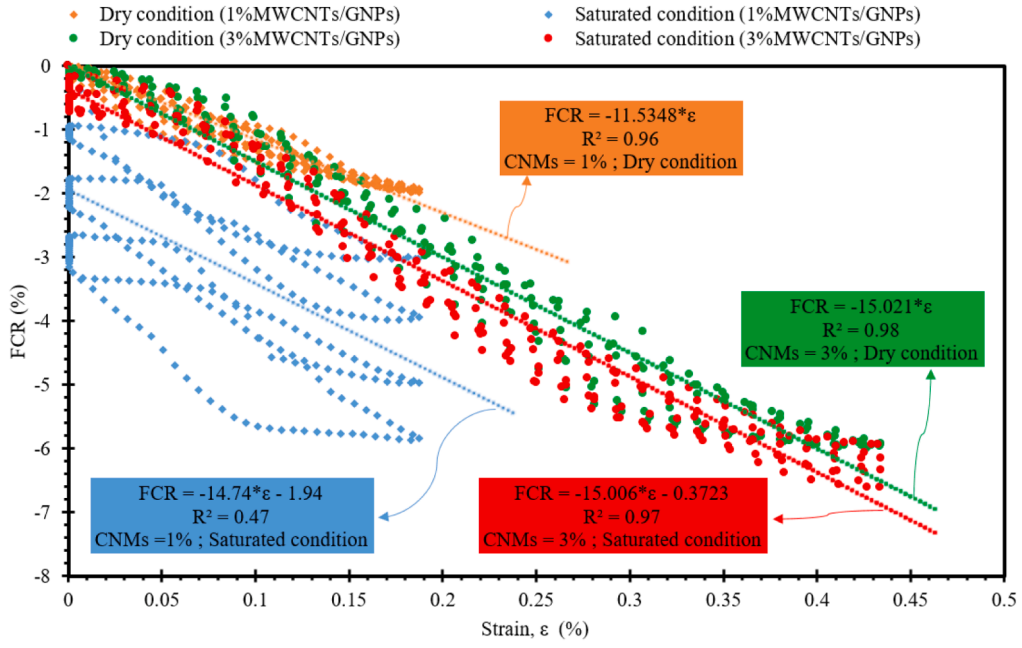
Fig. 19. Piezoresistive performance of 10% cement-stabilized sand under various degrees of saturation for specimens cured for 28-days: (a) specimens doped with 1% MWCNT/GNP, and (b) specimens doped with 3% MWCNT/GNP.

Piezoresistivity

Piezoresistive performance, which reflects the correlation between electrical resistance/resistivity/FCR and mechanical response (stress and strain), is one of the primary nonstructural functionalities of cement-stabilized sand infused with MWCNTs/GNPs. This property showcases how mechanical loading affects the FCR, with compressive loading leading to increased FCR (resulting from decreased electrical resistance) and unloading causing a decrease in FCR (due to increased electrical resistance). While the stress sensing, strain sensing, and damage sensing capabilities of cement-stabilized sand with MWCNTs/GNPs have been extensively studied in prior research by the authors in previous investigations [8,11,3], the current section is dedicated to exploring the influence of moisture content on the piezoresistive performance of cement stabilized sand. To this end, the piezoresistive performance of self-sensing cement-stabilized sand doped with 1 % MWCNTs/GNPs (at the lower limit of the percolation threshold) and 3 % MWCNTs/GNPs (at the upper limit of the percolation threshold) was examined under two conditions: a dry condition (zero degree of saturation) and fully saturated condition (100 % degree of saturation), as depicted in Fig. 19. Fig. 19a shows that self-sensing cement-stabilized sand doped with 1 % MWCNTs/GNPs exhibits two distinct patterns under cyclic compressive loading within the quasi-elastic region, depending on the moisture content. Under dry conditions (zero degree of saturation), the FCR under cyclic compressive loading shows no polarization. Conversely, under wet conditions (fully saturated condition), the FCR of self-sensing cement-stabilized sand doped with 1 % MWCNTs/GNPs under cyclic loading exhibits polarization effects. Under saturated conditions with self-sensing cement-stabilized sand containing 1 % MWCNTs/GNPs, ion migration significantly influenced polarization. However, this polarization effect is not significant for self-sensing cement-stabilized sand doped with 3 % MWCNTs/GNPs, as shown in Fig. 19b. In other words, when the MWCNTs/GNPs are within the



(a)



(b)

Fig. 20. Strain sensitivity of specimens cured for 28-days: (a) specimens doped with 1% MWCNT/GNP, and (b) specimens doped with 3% MWCNT/GNP.

percolation region, the movement of ions under saturated conditions does not significantly affect the electrical conductivity of cement-stabilized sand; instead, electron movement predominates. Consequently, the polarization effects caused by ion movement are not significant in the piezoresistive performance of cement-stabilized sand incorporating 3 % MWCNTs/GNPs, as shown in Fig. 19b. The findings obtained in this study are consistent with those in previous research in which self-sensing cementitious composites exhibited varying sensing performances with respect to moisture content [60]. To effectively utilize this self-sensing cement-stabilized sand in real-life projects in which moisture variation is prevalent, it is crucial to employ MWCNT/GNP concentrations higher than the lower limit of the percolation threshold.

To further assess the impact of self-sensing cement-stabilized sand on piezoresistive performance, the stress sensitivity (S) and strain sensitivity or G were analysed for specimens containing 1 % MWCNTs/GNPs and 3 % MWCNTs/GNPs. Fig. 20a illustrates the stress-sensing behaviour of cement-stabilized sand doped with 1 % MWCNTs/GNPs and 3 %

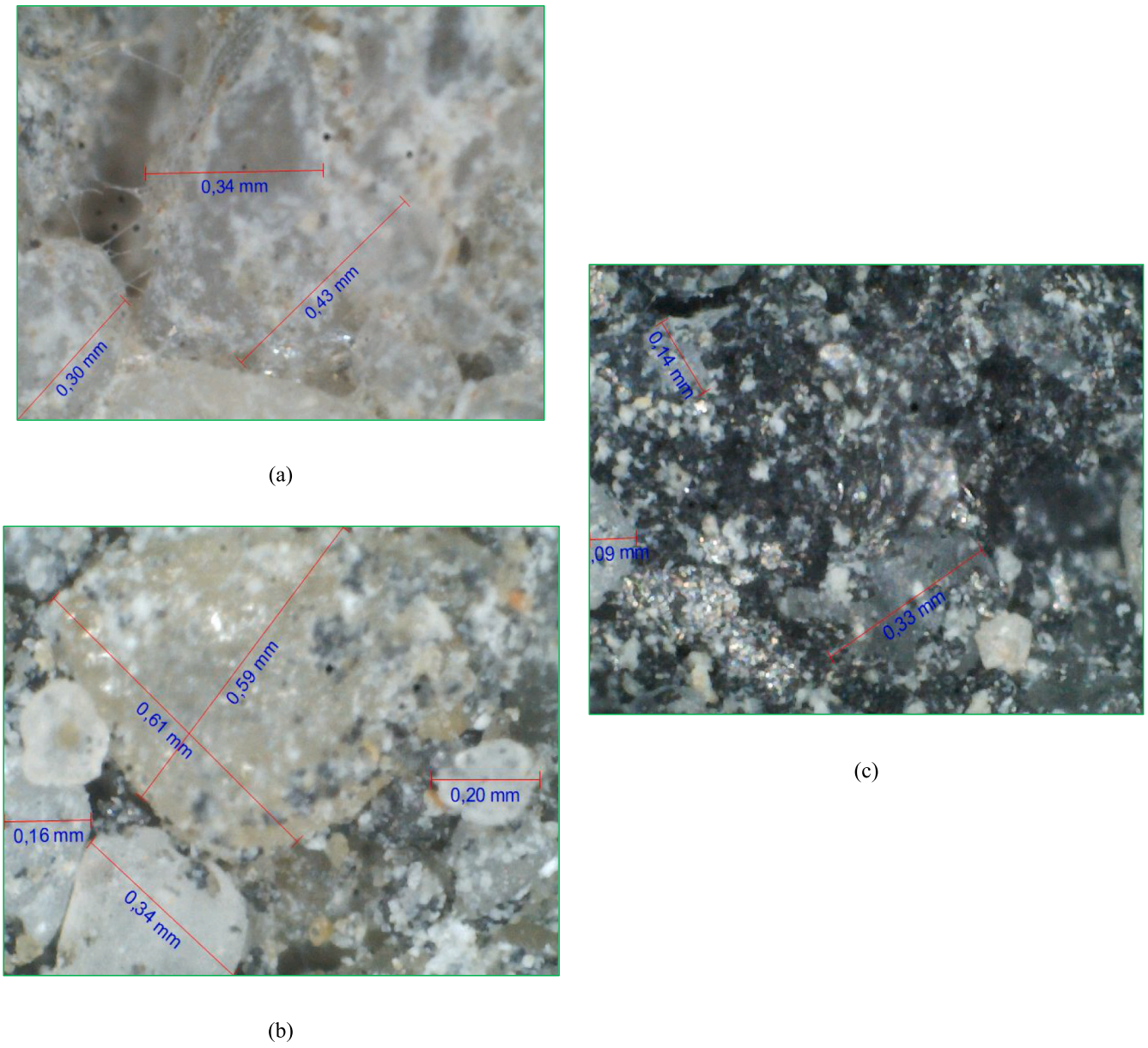


Fig. 21. Morphology of 10% cement-stabilized sand based on 400 magnification scale of micro camera for specimens cured for 28-days: (a) 0% MWCNT/GNP, (b) 0.5% MWCNT/GNP, and (c) 4% MWCNT/GNP.

MWCNTs/GNPs under both dry and saturated conditions. A comparison of the results depicted in Fig. 20a clearly demonstrates a significant decrease in the repeatability and linearity of the stress sensing performance in self-sensing cement-stabilized sand doped with 1 % MWCNTs/GNPs, accompanied by an increase in the hysteresis behaviour. This observed increase in hysteresis and decrease in linearity and repeatability of the self-sensing cement-stabilized sand doped with 1 % MWCNTs/GNPs under saturated conditions, as shown in Fig. 20a, can be attributed to the polarization or instability of electrical signals induced by ions movement, as discussed in Fig. 19a. Conversely, the influence of moisture on the stress-sensing performance of self-sensing cement-stabilized sand doped with 3 % MWCNTs/GNPs is negligible, as indicated in Fig. 20a. Fig. 20a reveals that there is no discernible difference in the linearity of the stress sensing performance between dry and wet conditions for self-sensing cement-stabilized sand doped with 3 % MWCNTs/GNPs. However, there is a slight decrease in repeatability under saturated conditions, as observed in Fig. 20a. The decreased effects of moisture on the stress sensing performance of self-sensing cement-stabilized sand doped with 3 % MWCNTs/GNPs, as shown in Fig. 20a, can be attributed to higher stability or lower polarization, as shown in Fig. 19b.

The strain sensitivity of self-sensing cement-stabilized sand can be assessed through the G (Equation (7). Fig. 20b presents the G of self-sensing cement-stabilized sand doped with 1 % MWCNTs/GNPs and 3 % MWCNTs/GNPs under dry and saturated conditions. Fig. 20b reveals that under dry conditions, the G increased from −11.53 for self-sensing cement-stabilized sand doped with 1 % MWCNTs/GNPs to −15.02 for those doped with 3 % MWCNTs/GNPs, indicating an increase in strain sensitivity with increasing percentage of MWCNTs/GNPs. The obtained G for self-sensing cement-stabilized sand doped with MWCNTs/GNPs are significantly greater than the G of commonly used strain gauges, which is usually approximately 2. However, the strain-sensing performance of self-sensing cement-stabilized sand can be influenced by moisture variation. For example, Fig. 20b illustrates the decreased linearity and repeatability of the strain sensing performance under wet conditions due to the hysteresis behaviour caused by polarization.

Although the G of self-sensing cement stabilized sand doped with 1 % MWCNTs/GNPs increased from −11.53 under dry conditions to −14.72 under saturated conditions, this increase is attributed to polarization (see Fig. 19a) caused by ions movement. Therefore, the increased G resulting from polarization is not reliable and may lead to considerable errors when implemented in real-life projects. To mitigate errors in the strain sensitivity performance of self-sensing cement-stabilized sand, it is essential to reduce hysteresis behaviour by increasing the concentration of conductive fillers. In this regard, the strain sensitivity of self-sensing cement-stabilized sand doped with 3 % MWCNTs/GNPs exhibited promising results under both dry and saturated conditions, as shown in Fig. 20b. Fig. 20b shows that the G of self-sensing cement-stabilized sand containing 3 % MWCNTs/GNPs remains nearly the same under both dry conditions (−15.01) and saturated conditions (−15). Moreover, Fig. 20b illustrates considerable repeatability and linearity for both dry and saturated conditions for cement-stabilized sand incorporating 3 % MWCNTs/GNPs. Additionally, the hysteresis behaviour of self-sensing cement-stabilized sand doped with 3 % MWCNTs/GNPs is negligible under wet conditions, as depicted in Fig. 20b.

Considering the obtained findings, it can be concluded that self-sensing cement stabilized sand doped with MWCNTs/GNPs within the percolation threshold range can yield reliable results. Although the findings of this study significantly facilitate the implementation of self-sensing cement-stabilized sand in the field, further investigations regarding the influence of moisture on the piezoresistive performance of self-sensing cement-stabilized sand are warranted.

Microstructure characteristics

The microstructure of cement-stabilized sand containing varying percentages of MWCNTs/GNPs was analyzed using a micro camera (Veho VMS-004 Discovery Deluxe), as depicted in Fig. 21. Fig. 21 provides insights into how MWCNTs/GNPs (conductive fillers) occupy the gaps and surfaces of sand particles. The infiltration of MWCNTs/GNPs into the gaps between sand particles disrupts the cementation bonding. For instance, in Fig. 21a, the cementation bonding formed by the cement hydration products between sand particles is visible. However, the introduction of MWCNTs/GNPs alters these cementation bonds, resulting in reduced mechanical strength due to weakened cementation bonding. As the concentration of MWCNTs/GNPs increases, the cementation bonding between sand particles weakens further. Additionally, Fig. 21 demonstrates that the rate of gap occupation increases with higher concentrations of MWCNTs/GNPs.

Noteworthy observations can be perceived from Fig. 21, indicating that the pore size between sand particles decreases with increasing percentages of MWCNTs/GNPs, leading to a denser microstructure. However, excessive infiltration of MWCNTs/GNPs into pores and voids hinders hydration production and weakens the cementation bonding between sand particles, resulting in diminished mechanical strength, as previously discussed in terms of resilient modulus. In general, it is important to highlight that while a very small amount of carbon nanomaterials may enhance mechanical strength, achieving piezoresistive performance in cement-stabilized sand requires a higher concentration of MWCNTs/GNPs. Consequently, this higher concentration of MWCNTs/GNPs contributes to the degradation of mechanical strength due to weakened cementation bonding caused by agglomeration and entanglement phenomena.

Moreover, the microstructural analysis reveals that the inclusion of MWCNTs/GNPs leads to the formation of conductive pathways, resulting in enhanced electrical conductivity, as depicted in Fig. 21. This figure demonstrates that the congestion of these pathways increases with higher concentrations of MWCNTs/GNPs. Consequently, a greater concentration of MWCNTs/GNPs corresponds to higher electrical conductivity. These formed conductive pathways contribute to the piezoresistive performance, which further improves with the increase in conductive pathways resulting from higher concentrations of MWCNTs/GNPs.

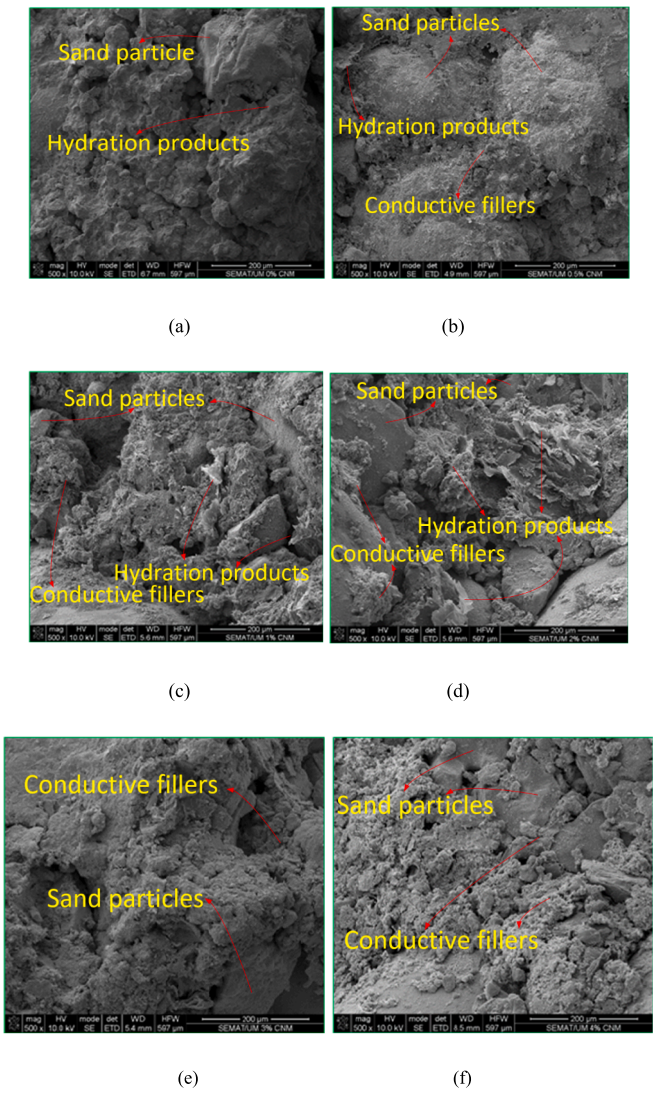


Fig. 22. Morphology of 10% cement-stabilized sand based on SEM experiment of specimens cured for 28-days: (a) 0% MWCNTs/GNPs, (b) 0.5% MWCNTs/GNPs, (c) 1% MWCNTs/GNPs, (d) 2% MWCNTs/GNPs, (e) 3% MWCNTs/GNPs (f), and 4% MWCNTs/GNPs.

Furthermore, the microstructural analysis conducted through SEM (SEM-FEG, Nano SEM NOVA 200, FEI) is depicted in Fig. 22. The SEM images offer similar insights as those obtained from the micro camera, as discussed previously. The cement hydration products (e.g., CSH, CAH) facilitate the cementation bonding between soil particles. However, the addition of excessive MWCNTs/GNPs in pursuit of achieving self-sensing cement-stabilized sand leads to the deterioration of the cementation bonding formed by cement hydration products. This degradation of cementation bonding intensifies with higher percentages of MWCNTs/GNPs, resulting in decreasing the resilient modulus, as discussed earlier. Analyzing the microstructure through both micro camera and SEM experiments reveals that MWCNTs/GNPs have a notable filling effect. Nevertheless, this filling effect is rendered ineffective due to the compromised cementation bonding. The entanglement of MWCNTs/GNPs particles absorbs the pore solution, consequently diminishing the cementation bonding.

Despite the microstructural analysis uncovering the degradation of cementation bonding resulting from the excessive incorporation of MWCNTs/GNPs, the mechanical strength obtained fell within the range specified by transportation geotechnical standards. Therefore, the self-

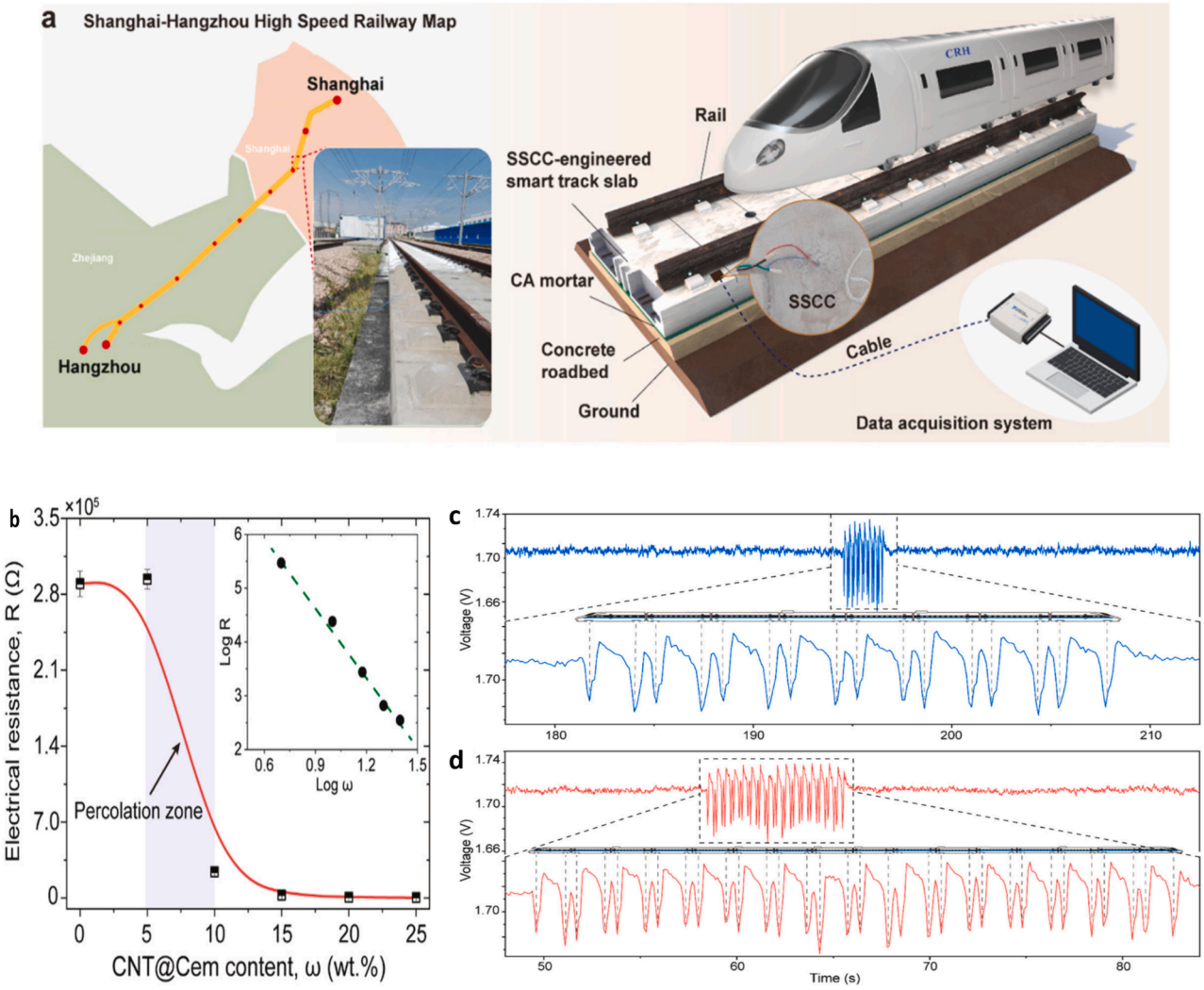


Fig. 23. (a) Application of self-sensing cementitious composites in slab tracks railways, (b) percolation threshold for producing self-sensing cementitious composite slab tracks, (c) voltage variation patterns of self-sensing cementitious composite slab tracks under 8-bogie trains, and (d) self-sensing cementitious composite slab tracks under 16-bogies trains [62].

sensing cement-stabilized sand developed in this study not only meets the mechanical requirements outlined in transportation geotechnical standards but also exhibits a nonstructural feature, namely self-sensing functionality, achieved through the addition of MWCNTs/GNPs.

Application of self-sensing cementitious composites in railway tracks

As previously mentioned, an extensive laboratory research program has investigated the piezoresistive capabilities of self-sensing cement-stabilized sands, notably through two EU projects: IN2TRACK and IN2TRACK3 (e.g., [3,8,9,10,11]), and recently referenced in the context of transportation geotechnics [61]. Despite plans to demonstrate its application on a section of the Portuguese railway network, this initiative has not yet materialized. In anticipation of future field applications, this section briefly explores examples of incorporating self-sensing cementitious composites into railway tracks, drawing from existing literature.

In this regard, the self-sensing cementitious composites produced using chemical vapour deposition (CVD) were installed in a high-speed railway (HSR) slab track network in China, as illustrated in Fig. 23a [62]. These self-sensing cementitious composites were created by incorporating 10 % in-situ-synthesized CNTs into cement (CNT@Cem) based on the percolation thresholds depicted in Fig. 23b. The voltage variation patterns under the passage of 8-bogie and 16-bogie trains over the self-sensing cementitious composite slab track are depicted in Fig. 23c and d. According to Fig. 23c and d, the voltage changes sharply upon the passage of train bogies, indicating the high performance of self-sensing cementitious composites produced using the CVD method. Observations presented in Fig. 23c and d suggest that the use of self-sensing cementitious composite slab tracks could be a promising approach for railway traffic monitoring, enabling train detection, axle counting, speed assessment, and identification of train types by analysing the number of sharp points in the voltage variation pattern.

Another application concerns a self-sensing railway sleeper developed that incorporates an array of fibre optic sensors for continuous monitoring under loading conditions [63]. Although this self-sensing sleeper, which employs fibre optic sensors, has demonstrated promising performance under loading, challenges exist, including limited longevity, high costs, localized measurement points, and maintenance difficulties [64]. To overcome the drawbacks associated with conventional sensors, an alternative approach involves fabricating self-sensing sleepers by incorporating 0.5 % CNTs, 0.75 % CNTs, and 1 % CNTs by weight of cement into conventional concrete sleepers. The fabrication and testing stages of these self-sensing sleepers are illustrated in Fig. 24 [65].

As previously discussed, wired-based instrumentation, including

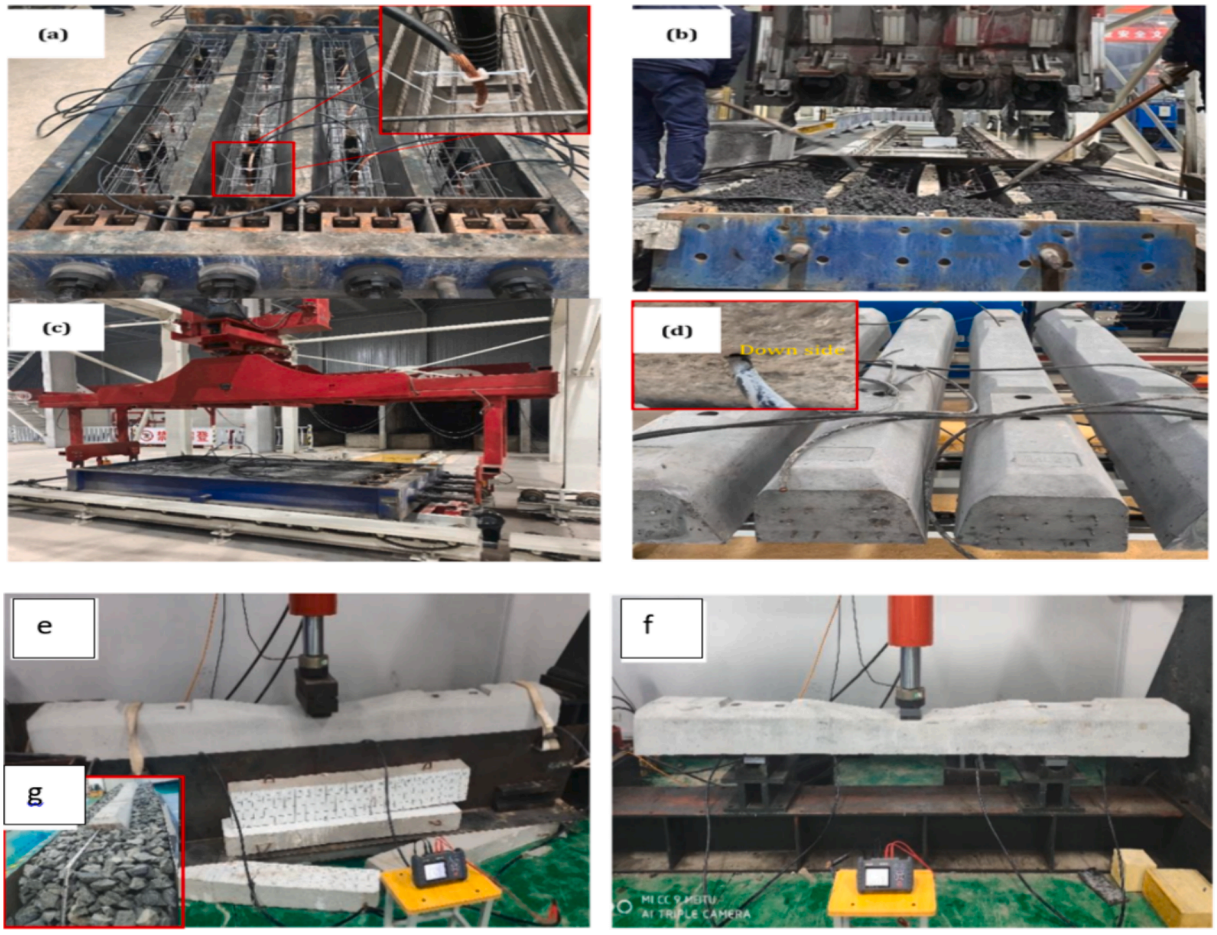


Fig. 24. Fabrication and testing setup of self-sensing cementitious sleepers doped with CNTs: (a) electrodes installation, (b) moulding, (c) vibration and curing, (d) manufactured self-sensing sleepers, (e) testing with full base support, (f) testing with two supports, and g) testing with ballast support [65].

wired self-sensing cementitious composites for traffic monitoring and SHM, has several limitations. Despite these challenges, self-sensing cementitious composites have been predominantly utilized in wired system configurations. However, there have been limited investigations aimed at transitioning self-sensing cementitious sensors from wired to wireless systems. For example, Le et al. [66] developed a wireless self-sensing cement-based sensor, doped with 1 % wt MWCNTs, by attaching a wireless signal transmitting device to the sensor and a wireless signal receiver at the data centre, as depicted in Fig. 25a. This wireless self-sensing cement-based sensor was successfully implemented in a railway sleeper, as shown in Fig. 25b.

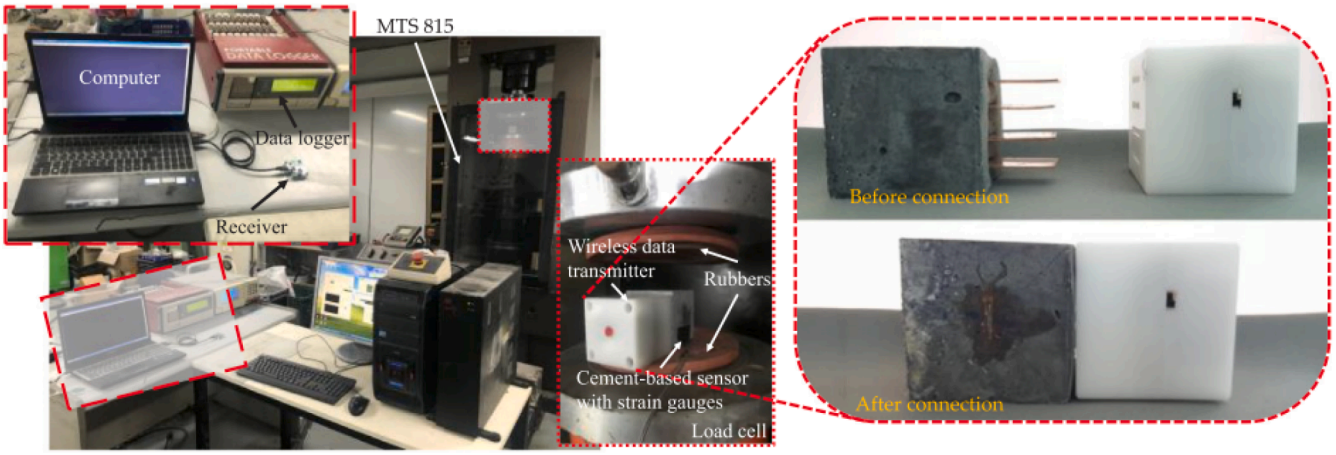
Although wireless sensors eliminate the need for wiring and associated maintenance work, the main concern remains the power supply required for the wireless sensor system [67]. Conventional wireless sensors typically rely on external power sources, such as batteries and solar systems. The challenges associated with replacing batteries and maintaining solar systems, along with the high costs involved, are significant drawbacks of conventional wireless sensors. However, the issue of power sourcing for sensors can be addressed by using self-powered sensors with energy harvesting devices [68]. These devices convert mechanical loading into a power source, thereby eliminating the need for external power. For example, a self-powered ZigBee sensor node was developed and employed in a railway track to convert vibrations into a power source [69].

Nevertheless, the incorporation of self-sensing cementitious composites provides a variety of benefits for rail track substructure structural integrity and maintenance. Indeed, while the inclusion of external sensors may weaken structures, self-sensing cementitious composites maintain structural strength while providing comprehensive sensing capabilities across the entire structure, rather than just localized areas typical of external sensor-based Structural Health Monitoring (SHM) systems. Furthermore, the continuous and autonomous monitoring facilitated by self-sensing cementitious composites improves reliability and allows for effective maintenance planning reducing life cycle costs of infrastructures. However, it is crucial to conduct detailed cost analyses comparing self-sensing cementitious composites with conventional alternatives in future research. To address cost concerns, exploring the mass production of carbon nanomaterials from waste materials emerges as a promising solution. This comprehensive approach not only highlights the benefits of self-sensing cementitious composites but also emphasizes the importance of strategic cost considerations and sustainable material sourcing in infrastructure development.

Conclusions

In this research, the impact of MWCNTs/GNPs was investigated on both the geotechnical and nonstructural properties (electrical resistance and piezoresistivity) of 10 % cement-stabilized sand. The following conclusions can be drawn based on the obtained findings:

Incorporating MWCNTs/GNPs into 10 % cement-stabilized sand led to a reduction in the $(\rho_d)_{max}$ and an increase in the OMC. However, the achieved compaction properties remained within the typical range used in the construction of transportation layers.



(a)



(b)

Fig. 25. (a) wireless self-sensing cement based sensor containing 1% MWCNTs [66], and (b) field setup [68].

The degree of saturation at the optimum moisture content (Sr)opt of cement-stabilized sand increased with increasing MWCNT/GNP percentages due to decreased $(\rho_d)_{max}$ and increased OMC.

The unified compaction curves exhibited a consistent trend on the right side of the peak point but differed on the left side. The uniform trend on the right side was attributed to better dispersion of MWCNTs/GNPs due to the higher water content, while the lack of uniformity on the left side was linked to agglomeration and entanglement challenges, possibly due to the lower water content.

The secant deformability modulus of cement-stabilized sand decreased as the concentration of MWCNTs/GNPs increased, indicating a decrease in the stiffness of the cement-stabilized sand.

The resilient modulus under cyclic compressive loading displayed an overall increasing trend, but beyond the quasi-elastic region, it decreased with increasing compressive loading.

The resilient modulus decreased with increasing percentages of MWCNTs/GNPs due to a degradation in cementation bonding between sand particles caused by agglomeration and entanglement.

The degradation curves of the resilient modulus showed a decreasing trend with increasing strain, with degradation increasing notably at higher MWCNT/GNP percentages.

The resilient modulus exhibited a decreasing trend with increasing degree of saturation (i.e., decreasing matric suction).

Electrical percolation analysis revealed an S-shaped curve correlating electrical conductivity with MWCNT/GNP concentration. The electrical conductivity significantly increased within the percolation threshold.

The influence of moisture on the electrical resistance of the cement-stabilized sand decreased with increasing MWCNT/GNP percentages. When the MWCNTs/GNPs exceeded the lower limit of the percolation threshold, the influence of saturation on the electrical resistance decreased substantially.

The established correlation between the resilient modulus and electrical resistance indicated a decreasing trend in the resilient modulus with decreasing electrical resistance.

Piezoresistivity analysis demonstrated that the effects of moisture on stress sensing and strain sensing of cement-stabilized sand decreased with increasing MWCNTs/GNPs.

Considering that the compaction parameters and resilient modulus fall within transportation standards, the use of MWCNTs/GNPs is recommended within the percolation threshold to produce well-performing multifunctional cement-stabilized sand. Despite a decrease in the mechanical properties of the geocomposites with increasing MWCNTs/GNPs, the resilient modulus obtained remained within the transportation standards.

While this paper provides insights into the geotechnical and piezoresistive characteristics of self-sensing cement-stabilized sand, there is still room for further studies to explore its structural and nonstructural properties under the complex stress and environmental conditions present in real rail track substructures.

Furthermore, the literature indicates the potential feasibility of employing self-sensing cementitious composites in railway track projects. It is believed that this novel geocomposite with self-sensing capabilities not only works as a conventional structural layer in the rail track substructure but also integrates a continuous monitoring system that exhibits significant advantages over previous conventional methods of monitoring the structural health of rail tracks. Such advancements align with the emerging era of intelligent structures, providing essential decision-making support for managers and operators alike.

CRediT authorship contribution statement

António Gomes Correia: Writing – review & editing, Writing – original draft, Visualization, Validation, Supervision, Project administration, Methodology, Investigation, Funding acquisition, Formal analysis, Data curation, Conceptualization. **Mohammad Jawed Roshan:** Writing – review & editing, Writing – original draft, Visualization, Validation, Methodology, Investigation, Formal analysis, Data curation, Conceptualization.

Declaration of competing interest

The authors declare that they have no known competing financial interests or personal relationships that could have appeared to influence the work reported in this paper.

Data availability

Data will be made available on request.

Acknowledgements

This work received partial support from the European Commission, Belgium, Shift2Rail Program under the project “IN2TRACK3, H2020–S2RJU-CFM-2020, S2R-CFMIP3- 01–2020”. Additionally, funding was provided by FCT / MCTES, Portugal, through national funds (PIDDAC), allocated to the R&D Unit Institute for Sustainability and Innovation in Structural Engineering (ISISE), Portugal, under reference UIDB / 04029/2020, project UID/QUI/00686/2020 of CQ, and the Associate Laboratory Advanced Production and Intelligent Systems ARISE, Portugal, under reference LA/P/0112/2020. Support was also received from the R&D Unit of the Centre for Textile Science and Technology (2C2T), Portugal. This research involved a multidisciplinary team and benefited from the active participation of many individuals. We extend our acknowledgments to Professor Raul Fangueiro from the Department of Textile Engineering, Professor Paulo Mateus Mendes from the Department of Industrial Electronics, and Professor Maria Manuela Silva from the Chemistry Department and Center of Chemistry, all from the University of Minho, Portugal. We also appreciate the contributions of Mohammadmahdi Abedi from the Civil Engineering Department at the University of Minho, Portugal, particularly in the original findings related to the IN2TRACK2 Project. Additionally, the second author acknowledges the individual research fellowship provided by the FCT, Portugal, with reference number “2023.03777.BD”.

References

[1] Roshan MJ, A Rashid AS, Abdul Wahab N, Tamassoki S, Jusoh SN, Hezmi MA, et al. Improved methods to prevent railway embankment failure and subgrade degradation: A review. Transp Geotech 2022;37:100834. Doi: 10.1016/j.trgeo.2022.100834.

[2] Razali R, Rashid ASA, Che Lat D, Horpibulsuk S, Roshan MJ, Rahman NSA, et al. Shear strength and durability against wetting and drying cycles of lime-stabilised laterite soil as subgrade. Phys Chem Earth, Parts A/B/C 2023;132:103479. https://doi.org/10.1016/j.pce.2023.103479.

[3] Jawed Roshan M, Abedi M, Gomes Correia A, Fangueiro R. Application of self-sensing cement-stabilized sand for damage detection. Constr Build Mater 2023;403:133080. https://doi.org/10.1016/j.conbuildmat.2023.133080.

[4] D'Alessandro A, Rallini M, Ubertini F, Materazzi AL, Kenny JM. Investigations on scalable fabrication procedures for self-sensing carbon nanotube cement-matrix composites for SHM applications. Cem Concr Compos 2016;65:200–13. https://doi.org/10.1016/j.cemconcomp.2015.11.001.

[5] Rana S, P S, Fangueiro R, Gomes Correia A. A review on smart self-sensing composite materials for civil engineering applications. AIMS Mater Sci 2016;3:357–79. Doi: 10.3934/matersci.2016.2.357.

[6] Dinesh A, Suji D, Pichumani M. Real-time implication of hybrid carbonaceous fibre and powder integrated self-sensing cement composite in health monitoring of beams and columns. Eur J Environ Civ Eng 2023;27:4563–80. https://doi.org/10.1080/19648189.2023.2194939.

[7] Abedi M, Fangueiro R, Gomes CA. A review of intrinsic self-sensing cementitious composites and prospects for their application in transport infrastructures. Constr Build Mater 2021;310:125139. https://doi.org/10.1016/j.conbuildmat.2021.125139.

[8] Roshan MJ, Abedi M, Gomes Correia A, Fangueiro R, Mendes PM. A Multifunctional Cementitious Composite for Pavement Subgrade. Materials (Basel) 2024;17:621. https://doi.org/10.3390/ma17030621.

[9] Roshan MJ, Abedi M, Gomes Correia A, Fangueiro R. Performance of Self-Sensing Cement-Stabilized Sand under Various Loading Conditions. Sensors 2024;24:1737. https://doi.org/10.3390/s24061737.

[10] Abedi M, Gomes Correia A, Fangueiro R. Geotechnical and piezoresistivity properties of sustainable cementitious stabilized sand reinforced with recycled fibres. Transp Eng 2021;6:100096. https://doi.org/10.1016/j.treng.2021.100096.

[11] Roshan MJ, Abedi M, Fangueiro R, Correia AG, Silva MM. Evaluation procedure for damage detection by a self-sensing cement composite. Measurement 2024;226:114149. https://doi.org/10.1016/j.measurement.2024.114149.

[12] Wang X, Cheng C, Zhang J, Ma G, Li J, Jin J. Real-time monitoring and quality assessment of subgrade compaction: key factors and ANN model. Acta Geotech 2023;18:3349–66. https://doi.org/10.1007/s11440-022-01769-1.

[13] Gomes CA. Soils mechanics in routine and advanced pavement and rail track rational design. Geotech roads, rail tracks earth Struct 2001:165–87.

[14] Gomes Correia A. Innovations in design and construction of granular pavements and railways. Adv. Transp. Geotech. – Ellis, Yu, McDowell, Dawson Thom, 2008, p. 17–28.

[15] Escobar A, Caicedo B, Cabrera M. Interaction between a cylinder and a partially saturated soil for compaction analysis. Transp Geotech 2021;30:100600. https://doi.org/10.1016/j.trgeo.2021.100600.

[16] Xu G, Chang GK, Wang D, Correia AG, Nazarian S. The pioneer of intelligent construction—An overview of the development of intelligent compaction. J Road Eng 2022;2:348–56. https://doi.org/10.1016/j.jreng.2022.12.001.

[17] Kodikara J, Islam T, Sounthararajah A. Review of soil compaction: History and recent developments. Transp Geotech 2018;17:24–34. https://doi.org/10.1016/j.trgeo.2018.09.006.

[18] Latimer R, Airey D, Tatsuoka F. Expected stiffness changes during compaction in laboratory and field. Transp Geotech 2023;43:101136. https://doi.org/10.1016/j.trgeo.2023.101136.

[19] Xu Z, Khabbaz H, Fatahi B, Wu D. Real-time determination of sandy soil stiffness during vibratory compaction incorporating machine learning method for intelligent compaction. J Rock Mech Geotech Eng 2022;14:1609–25. https://doi.org/10.1016/j.jrmge.2022.07.004.

[20] Tatsuoka F, Correia AG. Importance of Controlling the Degree of Saturation in Soil Compaction. Procedia Eng 2016;143:556–65. https://doi.org/10.1016/j.proeng.2016.06.070.

[21] Ying Z, Cui YJ, Benahmed N, Duc M. Salinity effect on the compaction behaviour, matric suction, stiffness and microstructure of a silty soil. J Rock Mech Geotech Eng 2021;13:855–63. https://doi.org/10.1016/j.jrmge.2021.01.002.

[22] Roshan MJ, Rashid ASBA, Bin HMA, Nejabi MN, Siti SN, Tamassoki S, et al. Evaluation of cement stabilised residual soil on macro- and micro-scale for road construction. J Eng Appl Sci 2022;69:109.. https://doi.org/10.1186/s44147-022-00165-6.

[23] Mengue E, Mroueh H, Lancelot L, Medjo ER. Evaluation of the Compressibility and Compressive Strength of a Compacted Cement Treated Laterite Soil for Road Application. Geotech Geol Eng 2018;36:3831–56. https://doi.org/10.1007/s10706-018-0576-x.

[24] Salahudeen AB, Eberemu AO, Osinubi KJ. Assessment of Cement Kiln Dust-Treated Expansive Soil for the Construction of Flexible Pavements. Geotech Geol Eng 2014; 32:923–31. https://doi.org/10.1007/s10706-014-9769-0.
[25] Biarez J, Gomes Correia A, Liu H, Taibi S. Stress-strain characteristics of soils interesting the serviceability of geotechnical structures. 2nd Int. Symp Pre-failure Deform Charact Geomaterials, Torino 1999:617–24.
[26] Coronado O, Caicedo B, Taibi S, Gomes Correia A, Souli H, Fleureau J-M. Effect of water content on the resilient behavior of non standard unbound granular materials. Transp Geotech 2016;7:29–39. https://doi.org/10.1016/j.trgeo.2016.04.004.
[27] Santos JA, Correia AG. Shear Modulus of soils under cyclci loading at small and medium strain level. Proc 12th World Conf Earthq Eng, Auckland, New Zealand 2000:1–8.
[28] Saberian M, Li J. Effect of freeze–thaw cycles on the resilient moduli and unconfined compressive strength of rubberized recycled concrete aggregate as pavement base/subbase. Transp Geotech 2021;27:100477. https://doi.org/10.1016/j.trgeo.2020.100477.
[29] Correia AG. Unbound granular materials : laboratory testing, in-situ testing and modelling. Proc. an Int. Work. Model. Adv. Test. unbound Granul.: Balkema, Rotterdam; 1999. p. 3–15.
[30] Roshan MJ, Rashid ASBA. Geotechnical characteristics of cement stabilized soils from various aspects: A comprehensive review. Arab J Geosci 2024;17:1. https://doi.org/10.1007/s12517-023-11796-1.
[31] Parveen S, Rana S, Fangueiro R, Paiva MC. Microstructure and mechanical properties of carbon nanotube reinforced cementitious composites developed using a novel dispersion technique. Cem Concr Res 2015;73:215–27. https://doi.org/10.1016/j.cemconres.2015.03.006.
[32] Abedi M, Fangueiro R, Camões A, Gomes CA. Evaluation of CNT/GNP's synergic effects on the Mechanical, Microstructural, and durability properties of a cementitious composite by the novel dispersion method. Constr Build Mater 2020; 260:120486. https://doi.org/10.1016/j.conbuildmat.2020.120486.
[33] Zhang L, Zheng Q, Dong X, Yu X, Wang Y, Han B. Tailoring sensing properties of smart cementitious composites based on excluded volume theory and electrostatic self-assembly. Constr Build Mater 2020;256:119452. https://doi.org/10.1016/j.conbuildmat.2020.119452.
[34] Deb K, Sawant VA, Kiran AS. Effects of fines on compaction characteristics of poorly graded sands. Int J Geotech Eng 2010;4:299–304. https://doi.org/10.3328/IJGE.2010.04.02.299-304.
[35] Taha MR, Alsharef JMA, Khan TA, Aziz M, Gaber M. Compressive and tensile strength enhancement of soft soils using nanocarbons. Geomech Eng 2018;16: 559–67. https://doi.org/10.12989/gae.2018.16.5.559.
[36] Tatsuoka F, Gomes CA. Importance of controlling the degree of saturation in soil compaction linked to soil structure design. Transp Geotech 2018;17:3–23. https://doi.org/10.1016/j.trgeo.2018.06.004.
[37] Biarez J, Correia AG, Lopez-Caballero F. From very small strains to failure. Deform Charact Geomaterials 2005:132–49.
[38] Silva J, Azenha M, Correia AG, Ferreira C. Continuous stiffness assessment of cement-stabilised soils from early age. Géotechnique 2013;63:1419–32. https://doi.org/10.1680/geot.13.P.021.
[39] Zhang J, Zhang A, Huang C, Yu H, Zhou C. Characterising the resilient behaviour of pavement subgrade with construction and demolition waste under Freeze-Thaw cycles. J Clean Prod 2021;300:126702. https://doi.org/10.1016/j.jclepro.2021.126702.
[40] Ding L qiang, Vanapalli SK, Zou W lie, Han Z, Wang X qun. Freeze-thaw and wetting-drying effects on the hydromechanical behavior of a stabilized expansive soil. Constr Build Mater 2021;275:122162. Doi: 10.1016/j.conbuildmat.2020.122162.
[41] Ardah A, Chen Q, Abu-Farsakh M. Evaluating the performance of very weak subgrade soils treated/stabilized with cementitious materials for sustainable pavements. Transp Geotech 2017;11:107–19. https://doi.org/10.1016/j.trgeo.2017.05.002.
[42] Gomes Correia A, Ramos A. A geomechanics classification for the rating of railroad subgrade performance. Railw Eng Sci 2022;30:323–59. https://doi.org/10.1007/s40534-021-00260-z.
[43] Gomes Correia A, AnhDan LQ, Koseki J, Tatsuoka F. Small strain stiffness under different isotropic and anisotropic stress conditions of two granular granite materials. Adv Lab Stress Test Geomaterials, Routledge 2018:209–15. https://doi.org/10.1201/9781315136776-11.
[44] Lee GC, Kim Y, Hong S. Influence of powder and liquid multi-wall carbon nanotubes on hydration and dispersion of the cementitious composites. Appl Sci 2020;10:1–13. https://doi.org/10.3390/app10217948.
[45] Shi T, Li Z, Guo J, Gong H, Gu C. Research progress on CNTs/CNFs-modified cement-based composites – A review. Constr Build Mater 2019;202:290–307. https://doi.org/10.1016/j.conbuildmat.2019.01.024.
[46] Zhang P, Su J, Guo J, Hu S. Influence of carbon nanotube on properties of concrete: A review. Constr Build Mater 2023;369:130388. https://doi.org/10.1016/j.conbuildmat.2023.130388.
[47] Indraratna B, Armaghani DJ, Gomes Correia A, Hunt H, Ngo T. Prediction of resilient modulus of ballast under cyclic loading using machine learning techniques. Transp Geotech 2023;38:100895. https://doi.org/10.1016/j.trgeo.2022.100895.
[48] Gomes Correia A, Cunha J. Analysis of nonlinear soil modelling in the subgrade and rail track responses under HST. Transp Geotech 2014;1:147–56. https://doi.org/10.1016/j.trgeo.2014.07.003.
[49] Correia AG, Barros JM de C, Santos JA dos, Niyama S. An Approach to Predict Shear Modulus of Soils in the Range of 10-6 to 10-2 Strain Levels. Int. Conf. Recent Adv. Geotech. Earthq. Eng. Soil Dyn., 2001.
[50] Vucetic M, Dobry R. Effect of Soil Plasticity on Cyclic Response. J Geotech Eng 1991;117:89–107. https://doi.org/10.1061/(ASCE)0733-9410(1991)117:1(89).
[51] Chen Q, Yu R, Li Y, Tao G, Nimbalkar S. Cyclic stress-strain characteristics of calcareous sand improved by polyurethane foam adhesive. Transp Geotech 2021; 31:100640. https://doi.org/10.1016/j.trgeo.2021.100640.
[52] Correia AG, Biarez J. Stiffness properties of materials to use in pavement and rail track design. Twelfth Eur. Conf. Soil Mech. Geotech Eng 1999:1245–50.
[53] Blackmore L, Clayton CRI, Powrie W, Priest JA, Otter L. Saturation and its effect on the resilient modulus of a pavement formation material. Geotechnique 2020;70: 292–302. https://doi.org/10.1680/jgeot.18.P.053.
[54] Han Z, Vanapalli SK. State-of-the-Art: Prediction of Resilient Modulus of Unsaturated Subgrade Soils. Int J Geomech 2016;16:1–15. https://doi.org/10.1061/(ASCE)GM.1943-5622.0000631.
[55] Zhang S, Ukrainczyk N, Zaoui A, Koenders E. Electrical conductivity of geopolymer-graphite composites: Percolation, mesostructure and analytical modeling. Constr Build Mater 2024;411:134536. https://doi.org/10.1016/j.conbuildmat.2023.134536.
[56] Han B, Yu X, Ou J. Sensing Mechanisms of Self-Sensing Concrete. Self-Sensing Concr. Smart Struct., Elsevier; 2014. p. 163–87.
[57] Lee HK, Nam IW, Tafesse M, Kim HK. Fluctuation of electrical properties of carbon-based nanomaterials/cement composites: Case studies and parametric modeling. Cem Concr Compos 2019;102:55–70. https://doi.org/10.1016/j.cemconcomp.2019.04.008.
[58] Gunn DA, Chambers JE, Uhlemann S, Wilkinson PB, Meldrum PI, Dijkstra TA, et al. Moisture monitoring in clay embankments using electrical resistivity tomography. Constr Build Mater 2015;92:82–94. https://doi.org/10.1016/j.conbuildmat.2014.06.007.
[59] Crawford MM, Bryson LS, Woolery EW, Wang Z. Using 2-D electrical resistivity imaging for joint geophysical and geotechnical characterization of shallow landslides. J Appl Geophys 2018;157:37–46. https://doi.org/10.1016/j.jappgeo.2018.06.009.
[60] Kim TU, Kim MK, Park JW, Kim DJ. Effects of temperature and humidity on self-stress sensing capacity of smart concrete blocks. J Build Eng 2023;69:106227. https://doi.org/10.1016/j.jobe.2023.106227.
[61] Kelly R, Indraratna B, Powrie W, Zapata C, Kikuchi Y, Tutumluer E, et al. State of the Art in Transportation Geotechnics. Proc. 20th ICSMGE-State Art Invit. Lect. Rahman Jaksa (Eds). Aust. Geomech. Soc. 2022, Sydney, Aust., 2022, p. 41–92.
[62] Ding S, Xiang Y, Ni YQ, Thakur VK, Wang X, Han B, et al. In-situ synthesizing carbon nanotubes on cement to develop self-sensing cementitious composites for smart high-speed rail infrastructures. Nano Today 2022;43:101438. https://doi.org/10.1016/j.nantod.2022.101438.
[63] Xu J, Butler LJ, Elshafie MZEB. Experimental and numerical investigation of the performance of self-sensing concrete sleepers. Struct Heal Monit 2020;19:66–85. https://doi.org/10.1177/1475921719834506.
[64] Elsherif M, Salih AE, Muñoz MG, Alam F, AlQattan B, Antonysamy DS, et al. Optical Fiber Sensors: Working Principle, Applications, and Limitations. Adv Photonics Res 2022;:3. https://doi.org/10.1002/adpr.202100371.
[65] Siahkouhi M, Wang J, Han X, Aela P, Ni YQ, Jing G. Railway ballast track hanging sleeper defect detection using a smart CNT self-sensing concrete railway sleeper. Constr Build Mater 2023;399:132487. https://doi.org/10.1016/j.conbuildmat.2023.132487.
[66] Lee SJ, Ahn D, You I, Yoo DY, Kang YS. Wireless cement-based sensor for self-monitoring of railway concrete infrastructures. Autom Constr 2020;119:103323. https://doi.org/10.1016/j.autcon.2020.103323.
[67] Alavi AH, Hasni H, Lajnef N, Chatti K. Continuous health monitoring of pavement systems using smart sensing technology. Constr Build Mater 2016;114:719–36. https://doi.org/10.1016/j.conbuildmat.2016.03.128.
[68] Salehi H, Burgueño R, Chakrabartty S, Lajnef N, Alavi AH. A comprehensive review of self-powered sensors in civil infrastructure: State-of-the-art and future research trends. Eng Struct 2021:234. https://doi.org/10.1016/j.engstruct.2021.111963.
[69] Gao M, Wang P, Wang Y, Yao L. Self-powered zigbee wireless sensor nodes for railway condition monitoring. IEEE Trans Intell Transp Syst 2018;19:900–9. https://doi.org/10.1109/TITS.2017.2709346.